Reactive oxygen species oxidize STING and suppress interferon production

Lili Tao[1], Andrew Lemoff[2], Guoxun Wang[1], Christina Zarek[1], Alexandria Lowe[1], Nan Yan[1,3], Tiffany A Reese[1,3]*

[1]Department of Immunology, University of Texas Southwestern Medical Center, Dallas, United States; [2]Department of Biochemistry, University of Texas Southwestern Medical Center, Dallas, United States; [3]Department of Microbiology, University of Texas Southwestern Medical Center, Dallas, United States

Abstract Reactive oxygen species (ROS) are by-products of cellular respiration that can promote oxidative stress and damage cellular proteins and lipids. One canonical role of ROS is to defend the cell against invading bacterial and viral pathogens. Curiously, some viruses, including herpesviruses, thrive despite the induction of ROS, suggesting that ROS are beneficial for the virus. However, the underlying mechanisms remain unclear. Here, we found that ROS impaired interferon response during murine herpesvirus infection and that the inhibition occurred downstream of cytoplasmic DNA sensing. We further demonstrated that ROS suppressed the type I interferon response by oxidizing Cysteine 147 on murine stimulator of interferon genes (STING), an ER-associated protein that mediates interferon response after cytoplasmic DNA sensing. This inhibited STING polymerization and activation of downstream signaling events. These data indicate that redox regulation of Cysteine 147 of mouse STING, which is equivalent to Cysteine 148 of human STING, controls interferon production. Together, our findings reveal that ROS orchestrates anti-viral immune responses, which can be exploited by viruses to evade cellular defenses.

Introduction

Reactive oxygen species (ROS) are reactive chemicals generated primarily in mitochondria as a byproduct of oxidative metabolism (*Schieber and Chandel, 2014*). Due to their capacity to inactivate DNA, proteins and lipids, ROS induce cell death and defend cells against many pathogens. However, accumulating evidence suggests that ROS also control cellular signaling pathways. ROS regulation of signal transduction allows cellular pathways to rapidly adapt to changes in the oxidative environment.

Even though some pathogens are effectively controlled by ROS, other pathogens thrive in a cellular environment where ROS are abundant (*Paiva and Bozza, 2014*). For instance, DNA viruses such as Kaposi's sarcoma associated herpesvirus (KSHV), herpes simplex virus-1 (HSV-1) and Epstein Barr virus (EBV), all induce oxidative stress in cells. Moreover, treatment with antioxidants such as N-acetyl-cysteine (NAC) reduces viral burden (*Paiva and Bozza, 2014*). In the case of herpesviruses, ROS not only enhance replication, but also induce virus reactivation from latency and potentially contribute to virally induced cancers (*Bottero et al., 2013*; *Chen et al., 2018*; *Gao et al., 2018*; *Gonzalez-Dosal et al., 2011*; *Ma et al., 2013*; *Ye et al., 2011*). The underlying mechanism for ROS promotion of virus replication and reactivation remains to be investigated. One possibility is that ROS regulate the signaling pathways that activate the immune response to these viruses, in particular, the DNA sensing pathways.

DNA normally localizes to the nucleus, and the presence of DNA in the cytosol serves as a universal danger signal to activate pattern recognition receptors (PRRs) that distinguish self from non-self. Upon virus infection, cytosolic DNA is recognized by DNA sensors such as cyclic GMP-AMP synthase

(cGAS), which catalyzes formation of an atypical cyclic di-nucleotide second messenger 2′,3′-cGAMP. 2′,3′-cGAMP binds and activates the Stimulator of Interferon Genes (STING) to induce production of type I interferon (IFN) and stimulate an immune response that promotes virus clearance (*Motwani et al., 2019*; *Wu and Chen, 2014*). Structural analysis of STING suggests that STING polymerization is necessary for its activation and that some cysteine residues may mediate STING polymerization by forming intermolecular disulfide bonds (*Ergun et al., 2019*; *Jin et al., 2010*; *Shang et al., 2019*). The chemical nature of cysteines is such that these residues are regulated by redox modifications, such as oxidation. However, post-translational modifications on STING cysteines have not been identified.

Because herpesviruses are DNA viruses that induce ROS and engage the cGAS/STING pathway, we hypothesized that ROS antagonize the production of interferon downstream of cGAS/STING during herpesvirus infection. Here, we found that ROS increased replication of murine gammaherpesvirus-68 (MHV68), a close genetic relative of KSHV and EBV. We also found that ROS suppressed interferon production in a STING-dependent manner. We further showed that the murine STING cysteine residue, C147 (equivalent to human C148), was oxidized upon ROS-inducing menadione treatment and that this cysteine was required for oxidation-sensitive inhibition of STING. Collectively, our results suggested that redox modification of STING is an important regulatory mechanism for STING activity during viral infection.

Results

ROS promote herpesvirus replication in macrophages

To determine if ROS promote a cellular environment conducive to virus replication, we used menadione as a tool to manipulate the level of ROS in cells. Menadione, also known as vitamin K3, is partially reduced by complex I in the mitochondria. The resulting semiquinone then participates in a redox cycle to partially reduce molecular oxygen, which generates ROS (*Iyanagi and Yamazaki, 1970*). Although prolonged treatment of a high dose of menadione leads to cell death, we determined a dose of menadione in bone marrow-derived macrophages (BMDMs) that induced no significant cell death (*Figure 1A*). Further, short-term treatment with menadione did not induce significant cell death even at a relatively high dose (*Figure 1A*). Menadione treatment is reported to reduce the glutathione/glutathione disulfide (GSH/GSSG) ratio and increase accumulated cellular ROS (*Chuang et al., 2002*; *Loor et al., 2010*). Consistent with these reports, we observed decreased gene expression of glutathione-disulfide reductase (*Gsr*) and glutamate-cysteine ligase regulatory subunit (*Gclm1*) with low-dose of menadione treatment. Therefore, menadione treatment of macrophages resulted in elevated oxidant levels in the cells (*Figure 1B*).

Because many viruses exploit ROS to facilitate their replication, we tested if increased ROS in macrophages affects growth of MHV68. To test the effects of ROS on virus replication, we first treated macrophages with low doses of menadione for sixteen hours, which increased cellular ROS while maintaining cell viability before virus infection. Macrophages were then infected with MHV68 at a multiplicity of infection (MOI) of 5 and virus growth was determined at indicated time points. Menadione treatment increased replication of MHV68 in a dose-dependent manner (*Figure 1C*). Hydrogen peroxide (H_2O_2) is a membrane permeable ROS, which induces secondary ROS production in cells upon extended treatment (*Fisher, 2009*). We pretreated macrophages with H_2O_2 at different concentrations for sixteen hours. The pretreatment was done in media containing FBS to maintain a cellular environment conducive to virus replication. We then infected macrophages with MHV68 at MOI of 5. Twenty-four hours after infection, cells expressing MHV68 lytic proteins were quantified using flow cytometry (*Reese et al., 2014*). Treatment with H_2O_2 increased the percentage of lytic protein positive cells in a dose-dependent manner (*Figure 1D*). Therefore, ROS induced by oxidants promoted MHV68 replication in macrophages.

ROS inhibit interferon response upon STING activation

We next determined whether ROS antagonized the antiviral response to promote herpesvirus replication. Because of the central role of interferons in controlling viral replication, we asked if ROS promoted MHV68 replication by inhibiting the interferon response. We first tested whether menadione treatment impacts virus growth in wildtype (WT) control macrophages and type I interferon receptor
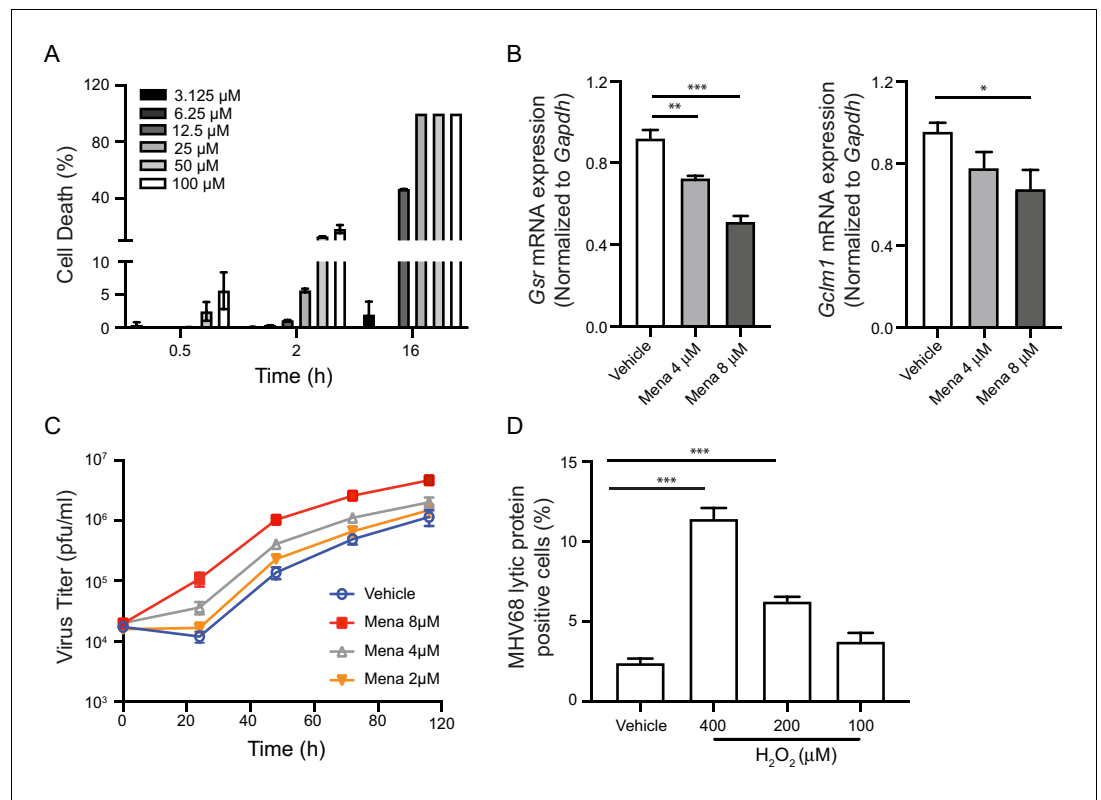
Figure 1. ROS promote herpesvirus replication in macrophages. (**A**) Fully differentiated bone marrow-derived macrophages (BMDMs) were treated with vehicle or different concentrations of menadione as indicated. Cell viability was determined at 0.5 hr, 2 hr and 16 hr after treatment. n = 2 with two technical repeats each time. (**B**) BMDMs were treated with vehicle, 4 μM or 8 μM menadione for 16 hr. Transcripts of *Gsr* and *Gclm1* were determined using qRT-PCR. n = 6. (**C**) BMDMs were treated with vehicle or different concentrations of menadione (mena) for 16 hr and then infected with MHV68 at multiplicity of infection (MOI) = 5. Virus titer was determined by plaque assay at 0 hr, 24 hr, 48 hr, 72 hr and 96 hr after infection. n = 3 with three technical repeats each time. (**D**) BMDMs were treated with vehicle or different concentrations of H_2O_2 for 16 hr in culture medium containing 10% fetal bovine serum, then infected with MHV68 at MOI = 5. Twenty-four hours after infection, cells were fixed and cells expressing virus lytic proteins were determined by flow cytometry. n = 3 with two technical repeats each time. Data are shown as mean ± SE, an ordinary one-way ANOVA was performed followed by Dunnett's multiple comparison test, only the p value for the most relevant comparisons are shown for simplicity. *, $p<0.05$, **, $p<0.01$, ***, $p<0.001$.

knockout ($Ifnar1^{-/-}$) macrophages (*Muller et al., 1994*). While menadione treatment robustly increased virus growth in WT macrophages, it did not increase virus growth in $Ifnar1^{-/-}$ macrophages, suggesting that menadione interfered with the interferon response during virus infection (*Figure 2A*). Consistent with this idea, macrophages treated with menadione had significantly fewer transcripts of *Ifnb* and interferon stimulated genes (ISGs), *Cxcl10, Ccl5, Isg20 and Isg15* (*Figure 2B and C*).

Because interferon responses are induced by multiple PRR signaling pathways after virus infection, we tested which PRR pathways were inhibited by ROS. Menadione treatment inhibited *Ifnb* expression upon interferon stimulatory DNA (ISD) stimulation, which engages the cGAS pathway. In contrast, menadione did not significantly alter the interferon response induced by poly I:C (sensed primarily by RIG-I) or poly dA:dT (sensed by multiple PRRs) (*Figure 2—figure supplement 1*). These results suggested that menadione-induced ROS selectively inhibited the cGAS-STING induced interferon response.

Sensing of cytosolic DNA involves the well-characterized cGAS signaling axis, which involves downstream components such as STING, TBK1 and IRF3. To further pinpoint which step of the
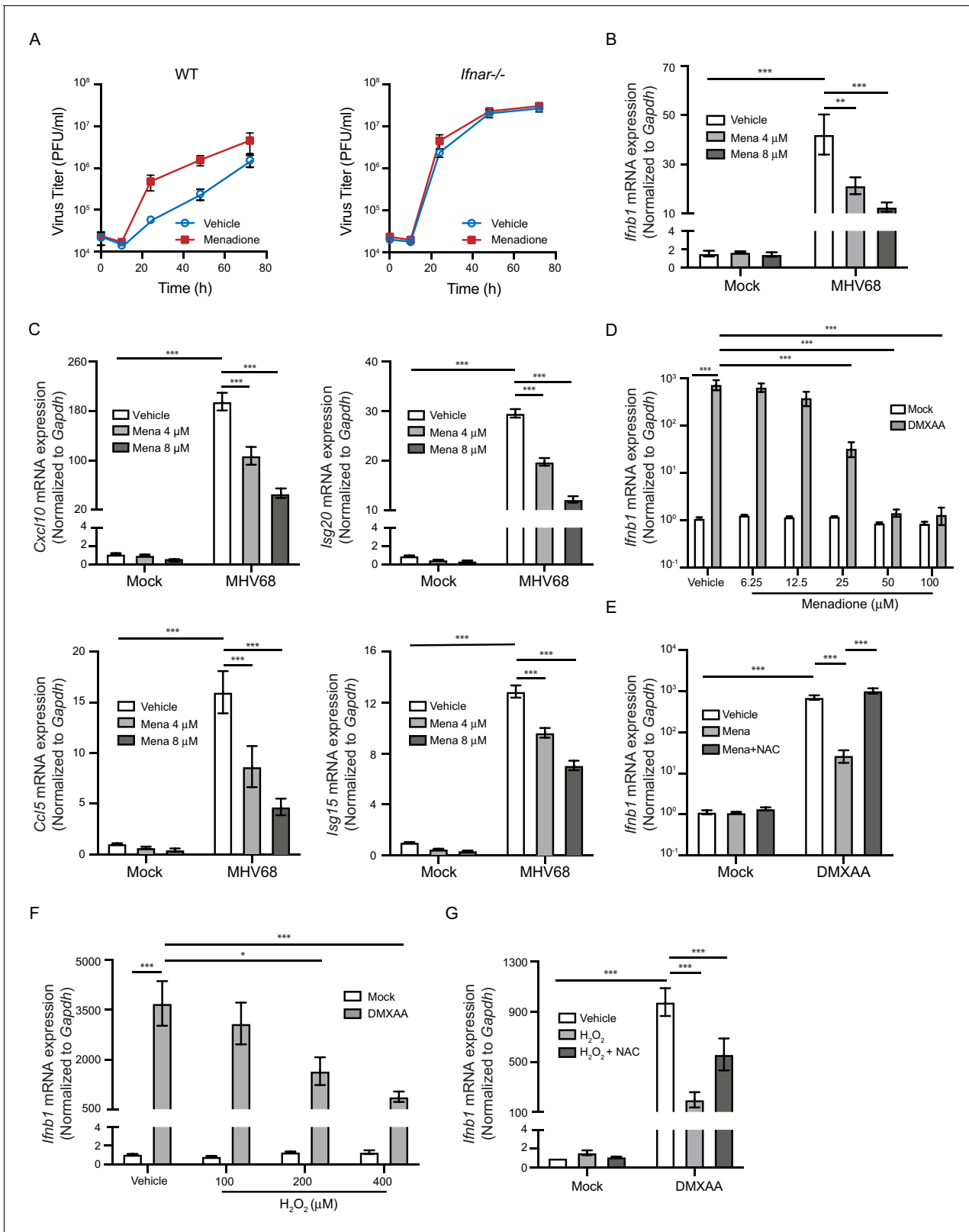
Figure 2. ROS inhibit interferon response upon STING activation. (**A**) BMDMs isolated from WT or *Ifnar-/-* mice were treated with vehicle or 8 μM menadione for 16 hr, then infected with MHV68 at MOI = 5. Virus titer was determined by plaque assay at 0 hr, 10 hr, 24 hr, 48 hr and 72 hr after infection. n = 1 with three technical repeats. (**B, C**) BMDMs were treated with vehicle, 4 μM or 8 μM menadione for 16 hr, then infected with MHV68 at MOI = 5. Transcripts of *Ifnb* (**B**) or ISGs (*Cxcl10, Isg20, Ccl5, Isg15*) (**C**) were determined at 6 hr after infection. n = 6. (**D**) BMDMs were treated with

Figure 2 continued on next page

Figure 2 continued

vehicle or different concentrations of menadione as indicated for 30 mins, then stimulated with DMXAA at 1 μg/ml. Transcripts of *Ifnb* were determined at 2 hr after stimulation. n = 3. (**E**) BMDMs were treated with vehicle, 25 μM menadione or 25 μM menadione and 2 mM NAC for 30 mins, then stimulated with 1 μg/ml DMXAA. Transcripts of *Ifnb* were determined at 2 hr after stimulation. n = 3. (**F**) BMDMs were treated with vehicle or different concentrations of H_2O_2 in serum free medium for 10 mins, then stimulated with 1 μg/ml DMXAA. Transcripts of *Ifnb* were determined 2 hr after stimulation. n = 3. (**G**) BMDMs were treated with vehicle, 200 μM H_2O_2 for 10 mins or 200 μM H_2O_2 for 10 mins followed by 5 mM NAC for 30 mins, then stimulated with 1 μg/ml DMXAA. Transcripts of *Ifnb* were determined 2 hr after stimulation. n = 4. Data are shown as mean ± SE, statistical analysis was conducted using two-way ANOVA followed by Tukey's multiple comparison test, only the p value for the most relevant comparisons are shown for simplicity. *, $p<0.05$, **, $p<0.01$, ***, $p<0.001$.

The online version of this article includes the following figure supplement(s) for figure 2:

Figure supplement 1. ROS regulate interferon response in macrophages upon STING activation.
Figure supplement 2. ROS regulate interferon response in macrophages upon STING activation with 2′,3′-cGAMP.
Figure supplement 3. ROS do not suppress interferon in primary fibroblasts.

cGAS-STING pathway is regulated by ROS, we directly induced STING activation with DMXAA and 2′,3′-cGAMP, two murine STING ligands. *Ifnb* expression induced by DMXAA and 2′,3′-cGAMP was strongly inhibited by different doses of menadione (***Figure 2D***, ***Figure 2—figure supplement 2***). Furthermore, treatment with the antioxidant N-acetyl-L-cysteine (NAC) restored *Ifnb* expression when combined with menadione (***Figure 2E***). To directly induce ROS in cells, we pulsed macrophages with H_2O_2 for 10 min prior to DMXAA stimulation. Similar to menadione treatment, H_2O_2 dose-dependently repressed transcription of *Ifnb* after DMXAA stimulation (***Figure 2F***). Addition of NAC after H₂O2 partially rescued *Ifnb* expression (***Figure 2G***). Collectively, these data suggest that ROS directly inhibited interferon production downstream of cGAS sensing.

Our next question was whether ROS inhibit interferon production in non-macrophage cell types. ROS production is a critical effector mechanism for macrophages to fend off microbial challenges (***Van Acker and Coenye, 2017***; ***Fang, 2011***). However, the high levels of ROS produced by macrophages requires the existence of intrinsic protective mechanisms against ROS, which otherwise would result in premature death of these immune cells during inflammatory responses. Indeed, macrophages are equipped with multiple mechanisms that allow them to be more resistant to ROS than other cell types (***Virág et al., 2019***). To test whether ROS inhibition of interferon production is a general immunoregulatory mechanism that functions in cells other than macrophages, we pulsed primary fibroblasts with H_2O_2 at the same concentration as we used in macrophages, followed by activation of STING with DMXAA. The expression of *Ifnb* in fibroblasts was not repressed, but rather slightly increased by H_2O_2 treatment (***Figure 2—figure supplement 3***). This is consistent with the notion that MEFs are more susceptible to ROS, which induces mitochondrial DNA fragmentation and primes interferon response (***West et al., 2015***). Therefore, ROS may negatively regulate interferon response in a cell-type and concentration dependent manner.

Endogenous ROS regulate interferon response

Because ROS are constantly generated by cellular respiration, cells contain low levels of ROS in the absence of exogenous stimulation. We therefore tested if endogenous ROS regulate the interferon response after STING activation. We first pretreated mouse macrophages with NAC to deplete endogenous ROS, then infected cells with MHV68. We observed elevated *Ifnb* and ISG expression with NAC treatment (***Figure 3A and B***). We also observed increased *Ifnb* transcripts when macrophages were cotreated with NAC and DMXAA, compared with DMXAA alone (***Figure 3C***). Peroxisomes are metabolically active organelles and are an important source of ROS in macrophages. ACOX1 is the rate-limiting enzyme that metabolizes long chain fatty acid in peroxisomes and is a major producer of H_2O_2. Using macrophages from *Acox1*^{-/-} mice (***Fan et al., 1996***), we observed increased *Ifnb* expression upon DMXAA stimulation compared to those isolated from the WT littermate controls (***Figure 3D***). We did not observe an inhibition in MHV68 virus growth by NAC pretreatment or in *Acox1*^{-/-} macrophages compared with wildtype (***Figure 3—figure supplement 1***). We speculate that the differences we observed in interferon levels caused by neutralizing basal ROS may not be sufficient to confer a viral growth difference, but these differences could be more
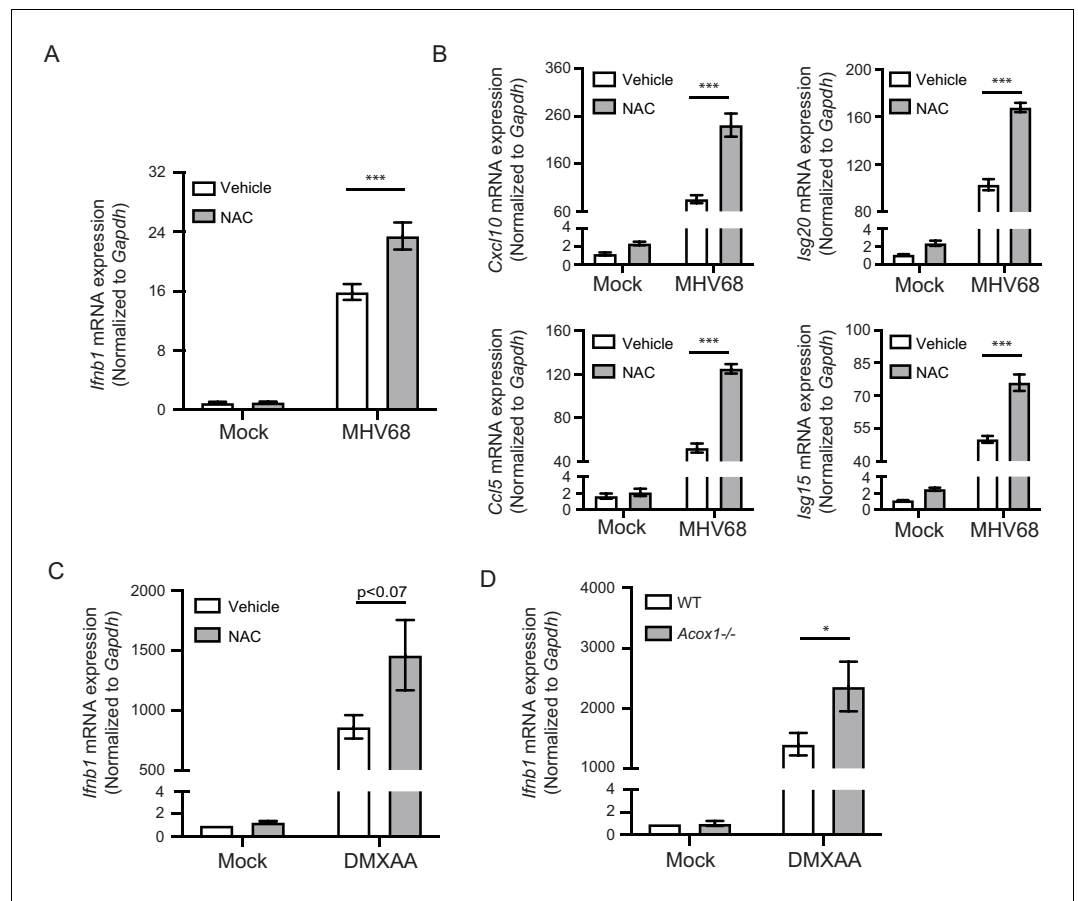
Figure 3. Endogenous ROS regulate interferon response upon STING activation. (**A, B**) BMDMs were treated with 2 mM NAC for 30 min, then infected with MHV68 at MOI = 5. Transcripts of *Ifnb* (**A**) or ISGs (*Cxcl10, Isg20, Ccl5, Isg15*) (**B**) were determined 6 hr after infection. n = 6. (**C**) BMDMs were treated with 2 mM NAC for 30 min, then stimulated with 1 μg/ml DMXAA. Transcripts of *Ifnb* were determined 2 hr after stimulation. n = 4. (**D**) BMDMs isolated from *Acox1-/-* or WT littermate control were stimulated with 1 μg/ml DMXAA. Transcripts of *Ifnb* were determined 2 hr after stimulation. n = 4. Data are shown as mean ± SE, statistical analysis was conducted using two-way ANOVA followed by Tukey's multiple comparison test, only the p value for the most relevant comparisons are shown for simplicity. *, p<0.05, **, p<0.01, ***, p<0.001.

The online version of this article includes the following figure supplement(s) for figure 3:

Figure supplement 1. Inhibition of endogenous ROS has no effect on virus replication.

significant in the context of a genetic background that predisposes to elevated interferon and autoimmunity.

ROS regulate interferon response by inhibiting STING polymerization

We next determined how ROS regulate STING-induced interferon production. STING is a transmembrane protein anchored on the endoplasmic reticulum (ER) as a dimer in the absence of stimulation. Upon activation, STING undergoes a conformational change and rearranges to form a polymer (*Ergun et al., 2019*; *Ishikawa et al., 2009*; *Tanaka and Chen, 2012*). It is then transported to the Golgi complex where it recruits TBK1, leading to TBK1 phosphorylation. STING also serves as a scaffolding protein to specify phosphorylation of IRF3 by phosphorylated TBK1 (pTBK1). Phosphorylated IRF3 (pIRF3) translocates to the nucleus and induces IFNβ transcription (*Wu and Chen, 2014*). To analyze activation of this pathway, we induced STING activation with DMXAA after treating BMDMs with H_2O_2 for 10 mins, and measured protein expression of STING, TBK1, and IRF3 at 0 mins, 30

mins, 60 mins and 90 mins after stimulation (*Figure 4A*). H_2O_2 treatment did not change the basal protein levels of STING, TBK1 or IRF3. However, pTBK1 and pIRF3 were significantly inhibited by H_2O_2 treatment. We also found that H_2O_2 inhibited TBK1 phosphorylation in a dose-dependent manner (*Figure 4B*). When using menadione to induce cellular ROS, pTBK1 and pIRF3 were also inhibited by menadione treatment (*Figure 4C*). These data suggest ROS inhibit interferon signaling upstream of TBK1 activation, possibly by inhibiting STING activation.

Next, we measured herpesvirus growth to test whether STING is required for the inhibitory effect of ROS on interferon. To this end, we quantified virus growth in WT and STING-deficient macrophages (*Sauer et al., 2011*). Menadione increased virus growth in WT macrophages but had no effect on virus growth in STING-deficient macrophages, supporting our hypothesis that ROS inhibited interferon in a STING-dependent manner (*Figure 4D*).

We subsequently determined if polymerization of STING was regulated by ROS, because STING polymerization is an early event in STING activation that occurs prior to translocation to the ER. In the absence of stimulus, STING monomers spontaneously form dimers. This process does not involve covalent linkage between the monomers. In contrast, STING polymerization requires the formation
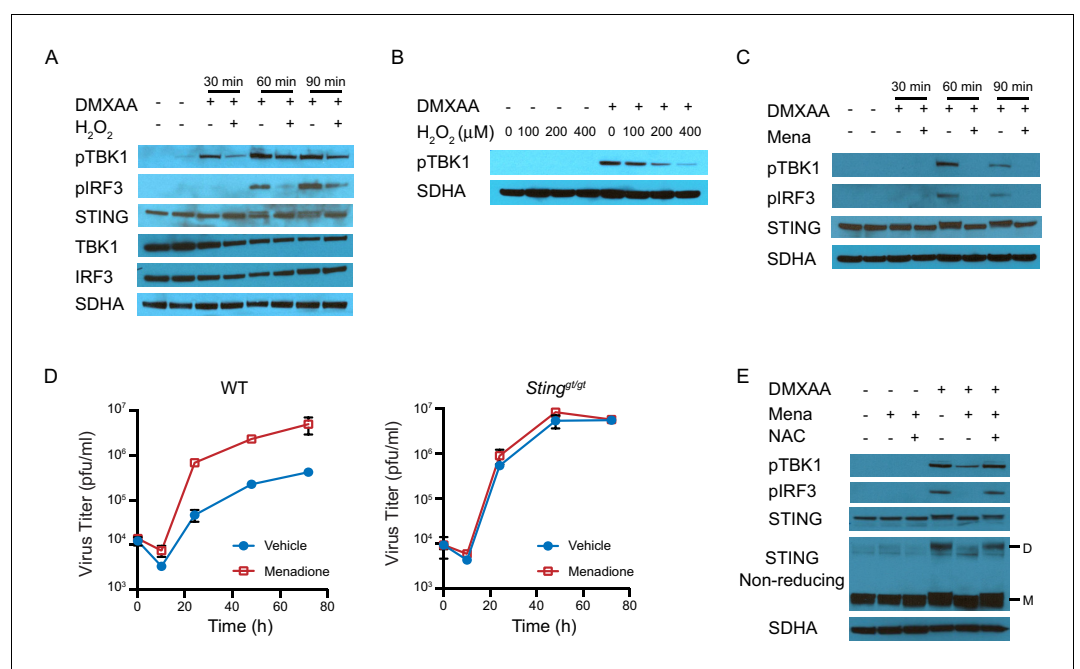

Figure 4. ROS regulate interferon response by inhibiting STING dimerization. (**A**) BMDMs were treated with vehicle or 200 µM H_2O_2 for 10 min in serum free culture medium, then stimulated with 1 µg/ml DMXAA. Western blots of TBK1, IRF3, STING, pTBK1 and pIRF3 were performed at 0 min, 30 min, 60 min and 90 min after stimulation. Data shown are representative of 2 independent experiments. (**B**) BMDMs were treated with vehicle or different concentrations of H_2O_2 in serum free culture medium for 10 mins, then stimulated with 1 µg/ml DMXAA. Level of pTBK1 was determined at 60 min after stimulation. n = 1 (**C**) BMDMs were treated with vehicle or 25 µM menadione for 30 min, then stimulated with 1 µg/ml DMXAA. Western blot of TBK1, IRF3, STING, pTBK1 and pIRF3 was performed at 0 min, 30 min, 60 min and 90 min after stimulation. Data shown are representative results of two independent experiments. (**D**) BMDMs isolated from WT control or *Sting$^{gt/gt}$* mice were treated with vehicle or 8 µM menadione for 16 hr, then infected with MHV68 at MOI = 5. Virus titer was determined by plaque assay at 0 hr, 10 hr, 24 hr, 48 hr and 72 hr after infection. n = 3 with three technical repeats each time. (**E**) BMDMs were treated with vehicle, 25 µM menadione, 25 µM menadione and 2 mM NAC for 30 min, then stimulated with 1 µg/ml DMXAA. STING polymerization was determined by non-reducing SDS-PAGE. M: STING monomer; D: STING dimer. Data shown are representative of 2 experiments.

The online version of this article includes the following figure supplement(s) for figure 4:

Figure supplement 1. Schematic diagrams of STING monomer, dimer and polymer on different electrophoresis gels.

Figure supplement 2. ROS decrease TBK1 recruitment during STING activation.

of interdimer disulfide bonds (*Ergun et al., 2019*). Therefore, polymerized STING appears as a dimer on non-reducing SDS-PAGE, as SDS disrupts only the non-covalent interactions, leaving covalent disulfide bonds between the monomers intact (*Figure 4—figure supplement 1*). As expected, DMXAA induced STING polymerization (shown as a dimer) and phosphorylation of TBK1 and IRF3. However, polymerization was significantly inhibited by menadione treatment, and restored by the addition of NAC (*Figure 4E*). As a result of decreased STING polymerization, the recruitment of TBK1 upon DMXAA stimulation was also diminished (*Figure 4—figure supplement 2*). In conclusion, ROS regulate interferon signaling by inhibiting STING polymerization.

ROS oxidization of STING at Cysteine-148 blocks STING activation

The next question we addressed was whether ROS oxidized STING, thus inhibiting polymerization. Recent structural studies suggest that STING polymerization and activation require formation of an intermolecular disulfide bond at Cysteine 148 (*Ergun et al., 2019*). The ability of C148-C148 disulfide bonds to bridge STING dimers suggests that the residue harbors a free thiol prior to stimulation. Because free thiol functional groups are susceptible to oxidation, we hypothesized that ROS inhibit STING function by oxidizing this free thiol group. To test this hypothesis, we treated human STING (hSTING) overexpressing fibroblast cells with menadione or hydrogen peroxide, followed by labeling of free thiols on STING with 5-iodoacetamido-fluorescein (5-IAF) in cell lysate. We then immunoprecipitated STING protein and blotted for STING and fluorescein (FITC). Treatment with either menadione or H_2O_2 decreased the level of free thiols on STING, measured as decreased FITC signal relative to STING protein (*Figure 5A*). In addition, we treated mouse macrophages with diamide, a reagent that specifically oxidizes free thiols to form disulfide bonds (*Kosower and Kosower, 1995*). Although diamide treatment induced formation of the STING polymer, such polymers were likely not functional because STING activation requires ligand-induced conformational change (*Shang et al., 2019*). This was consistent with our observation that diamide treated macrophages failed to phosphorylate TBK1 and upregulate *Ifnb* upon DMXAA stimulation (*Figure 5B and C*). Thus, ROS oxidized free cysteine(s), thereby blocking the activation of both overexpressed human STING and endogenous mouse STING.

To identify the precise site of modification on STING, we labeled both reduced and oxidized cysteines with iodoacetamide (IAM) and N-ethylmaleimide (NEM) on STING. First, we treated mouse macrophages with vehicle control or menadione. This was followed by alkylation of free thiols by IAM, labeling reduced cysteines (Cys_red). We then immunoprecipitated STING, reduced oxidized thiols, and alkylated the DTT-reduced thiol groups with NEM, labeling oxidized cysteines (Cys_ox). We lastly quantified the ratio of IAM (identified as Carbamidomethylation, CAM)/NEM modification on specific cysteines using liquid chromatography with tandem mass spectrometry (LC-MS/MS) (*Figure 5D*; *Wu et al., 2020*). By this effort, we determined that C147 of endogenous murine STING was modified by both CAM and NEM (*Figure 5—figure supplement 1*). While very low levels of NEM modification (Cys_ox) were detected on C147 of endogenous murine STING in vehicle-treated sample, approximately one quarter of C147 was modified by NEM with menadione treatment, indicating increased oxidation of C147 (*Figure 5E and F*). This cysteine residue is highly conserved across all mammalian species (*Figure 5—figure supplement 2*) and is critical for STING function. C147 in mouse is equivalent to C148 in human STING. A C148A mutant of hSTING is unable to form an intermolecular disulfide bond and induce interferon response upon stimulation (*Ergun et al., 2019*). To confirm the critical role C148 in STING polymer formation, we treated 293 T cells overexpressing a C148A mutant of hSTING with diamide. While diamide induced formation of polymer on WT STING, we observed significantly less polymer formation with diamide on the C148A mutant (*Figure 5G*). Altogether, we propose that C147 on murine STING and C148 on human STING are oxidized by ROS, thereby blocking STING activation.

ROS regulate MHV68 replication in vivo

We have shown in vitro that ROS regulate interferon induction; however, whether this regulation is physiologically important remains to be investigated. To address this question, we either induced ROS with menadione or inhibited endogenous ROS with NAC in mice. We then infected mice with a luciferase tagged-MHV68 reporter virus and monitored acute replication of the virus by luciferase signal (*Figure 6A*; *Hwang et al., 2008*; *Reese et al., 2014*). Treatment of mice with 10 mg/kg
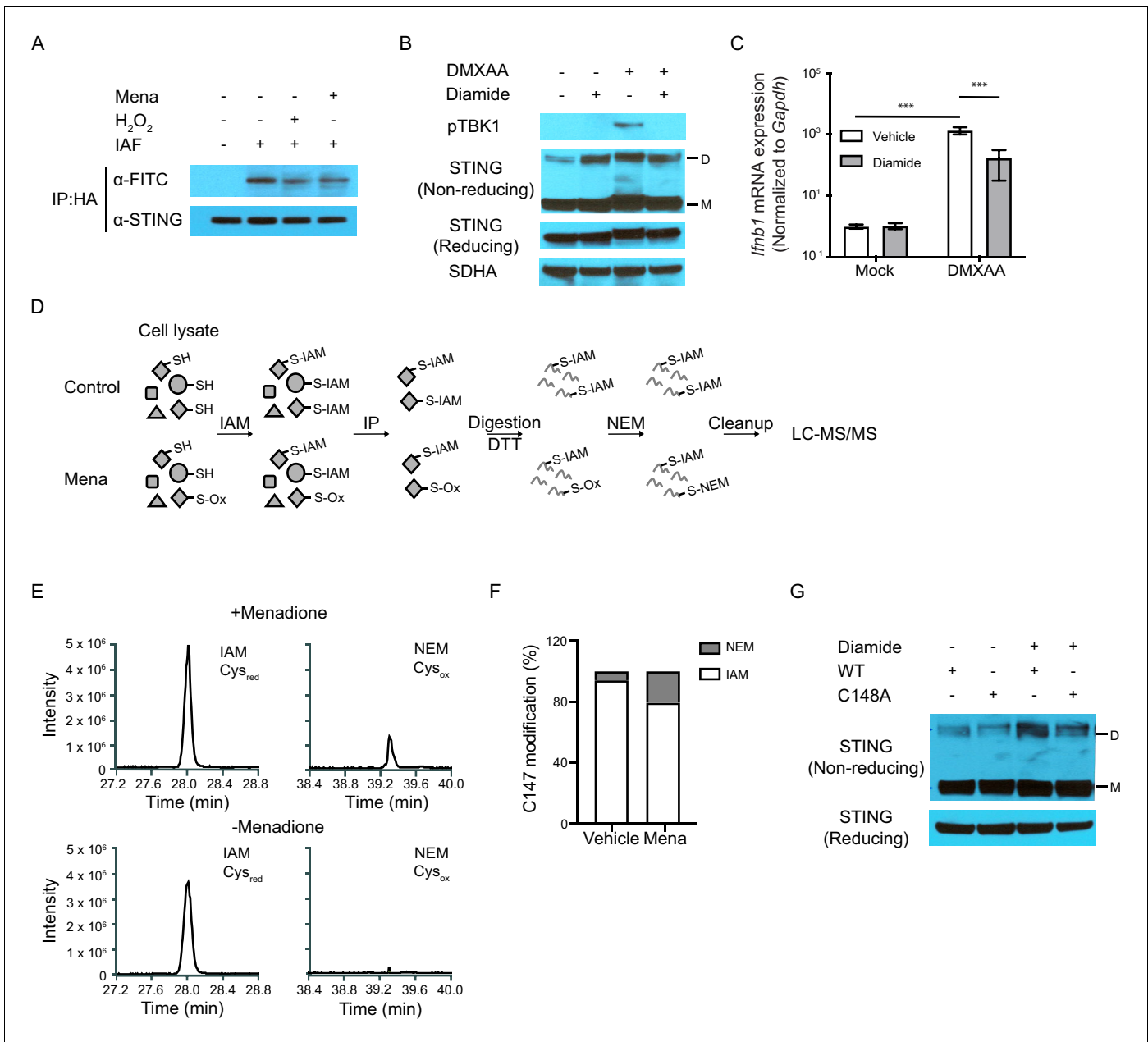
Figure 5. ROS oxidize C148 on STING. (**A**) *Sting-/-* fibroblasts stably expressing HA-tagged human STING were treated with vehicle or 200 µM H_2O_2 in serum free medium for 10 min. Cell lysates were incubated with 5 µM 5-IAF for 1 hr at room temperature to label free thiols. Protein levels of STING and FITC were detected after immunoprecipitation for HA-tagged protein. Data shown are representative results of two independent experiments. (**B, C**) BMDMs were treated with 200 µM diamide for 30 mins. STING polymers (B, n = 2) and *Ifnb* transcripts (C, n = 4) were determined at 1 hr after 1 µg/ml DMXAA stimulation. M: STING monomer; D: STING dimer. Bars represent the mean ± SE, *p* value was calculated using two-way ANOVA followed by Tukey's multiple comparison test. Only the *p* values for the most relevant comparison are shown for clarity purpose. ***, p<0.001. (**D**) Schematic of differential alkylation (IAM labeling followed by DTT reducing and NEM labeling) of cysteines for mass spectrometry analysis. (**E**) Mass spectra of IAM- and NEM-modified STING in vehicle and menadione treated samples. n = 1 (**F**) Quantification of Cys_{red} and Cys_{ox} from mass spectrometry analysis. (**G**) Vectors with WT STING or C148A mutated STING were transfected into HEK293T cells. Twenty-four hours after transfection, cells were treated with vehicle or 200 µM diamide for 30 min. Polymer of STING was determined with non-reducing SDS-PAGE. M: STING monomer; D: STING dimer. n = 1. The online version of this article includes the following figure supplement(s) for figure 5:

Figure supplement 1. Representative MS/MS spectra of $SAVC_{147}EEK$ peptide in STING protein modified by both IAM (CAM) and NEM.
Figure supplement 2. Sequence alignment of STING from multiple species suggested C148 of STING is highly conserved across mammalian species.
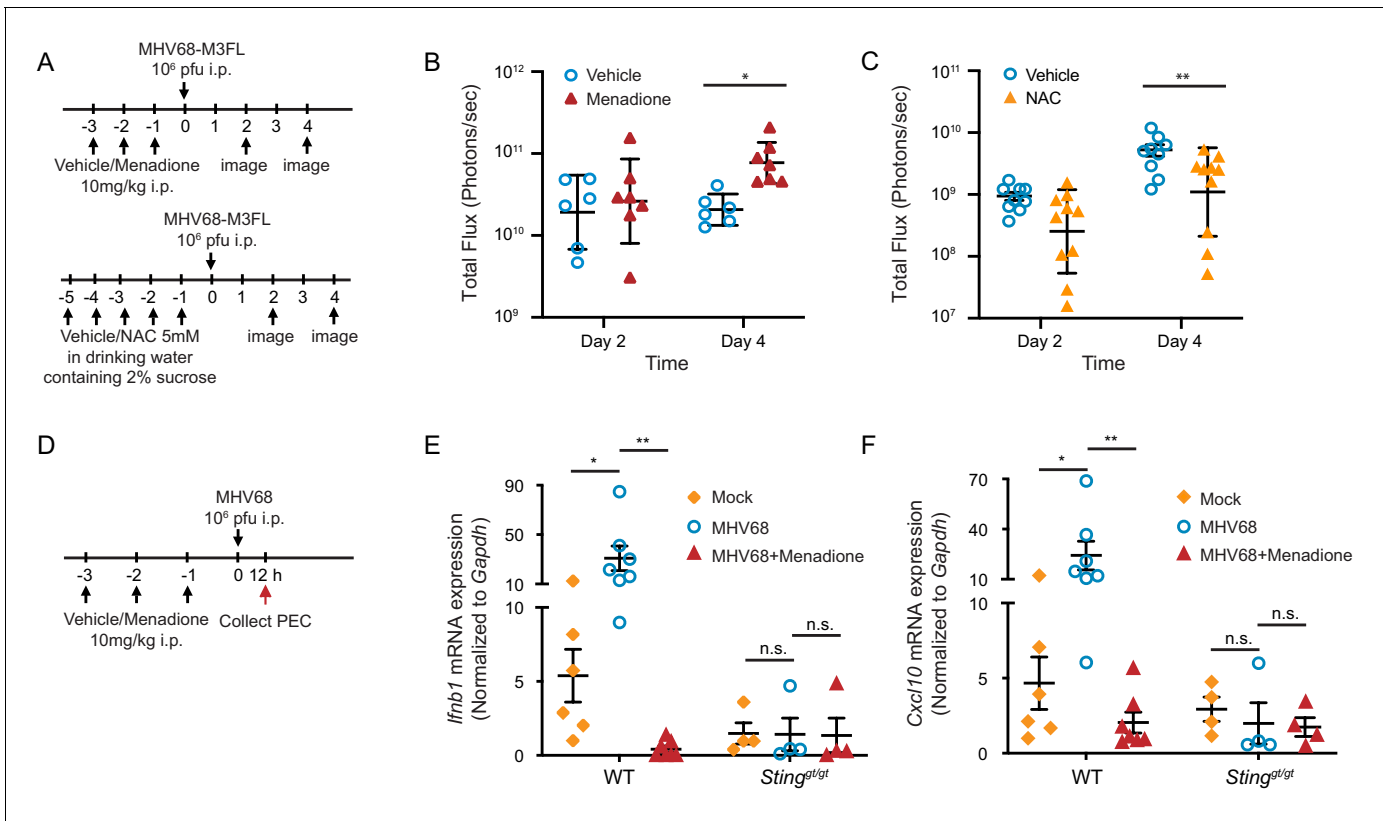
Figure 6. ROS regulate MHV68 replication in vivo. (A) Schematic of MHV68 replication in mice with menadione treatment or NAC treatment. (B, C) 8–12 weeks old mice were sex-matched and randomly assigned to groups prior to experiment. Mice were treated and infected as shown in (A). Total flux (photons/second) was measured using IVIS bioluminescence imager at day 2 and day 4 after infection to quantitate lytic replication of MHV68. Data shown were the results obtained from a pool of two independent experiments. Bars represent geometric mean ±geometric SD. Each dot represents an individual mouse. (D) Schematic for the quantification of interferon and ISG transcripts in mice with menadione treatment during MHV68 infection. 7–12 weeks old mice were sex-matched and randomly assigned to groups prior to experiment. Mice were treated with either vehicle control (5% DMSO in corn oil) or menadione (10 mg/kg in corn oil) for 3 days, then infected with 10^6 PFU MHV68 peritoneally. Twelve hours post infection, transcripts of *Ifnb* and *Cxcl10* in peritoneal exudate cells (PECs) were determined from individual mice. (E, F) Transcripts of *Ifnb* and *Cxcl10* in PECs from mock (vehicle treatment, no infection), MHV68 (vehicle treatment, MHV68 infected) and MHV68+Menadione (Menadione treatment, MHV68 infected) mice. Bars represent mean ± SE, each dot represent an individual mouse. Data are collected from one controlled experiment. Statistical analysis was conducted using two-way ANOVA (repeated measures). *p<0.05.

menadione increased virus replication (*Figure 6B*). In contrast, treatment of mice with NAC inhibited virus replication (*Figure 6C*). Additionally, we measured the interferon response in both WT and *Sting^{gt/gt}* mice during MHV68 infection (*Figure 6D*). While expression of *Ifnb1* and *Cxcl10* was increased in peritoneal exudate cells 12 hr after virus infection in WT mice, such response was diminished in *Sting^{gt/gt}* mice. Consistent with our in vitro data, menadione treatment dramatically inhibited interferon and ISG production induced during MHV68 infection (*Figure 6E and F*). These data suggest that ROS are important for controlling virus replication in vivo.

Discussion

Recent work indicates that ROS regulate cellular defense pathways, including Toll-like receptor signaling and inflammasome activation (*Bulua et al., 2011*; *Schieber and Chandel, 2014*; *Soucy-Faulkner et al., 2010*; *Tschopp and Schroder, 2010*; *West et al., 2011*). However, the function of ROS in DNA sensing pathways has not been investigated. Here, we found that ROS regulate cytoplasmic DNA sensing by inhibiting STING activity during herpesvirus infection. ROS suppressed the activation of STING, as well as the activation of TBK1 and IRF3, thus leading to reduced IFNβ

transcription. Importantly, we also determined that ROS oxidized a particular cysteine residue, C147, of murine STING. When we mutated the equivalent human C148 residue, diamide was no longer able to oxidize STING and form functional polymers, suggesting that redox regulation of STING required this cysteine residue. We also explored the functional consequence of ROS regulation of STING activity in vivo and demonstrated that treatment of mice during herpesvirus infection with either an inducer of ROS or a neutralizer of ROS, increased or decreased MHV68 replication in mice, respectively. Consistent with these findings, a ROS inducer inhibited interferon production during herpesvirus infection in a STING dependent manner. Our work suggests that redox modification of STING is an important mechanism for regulating STING activity, which may explain how herpesviruses manipulate STING signaling and reduce interferon levels to support their replication. Notably, elevated ROS levels in the context of viral infection is of high clinical relevance, as ROS is increased in elderly people as well as in many diseases, including cardiovascular diseases, lung fibrosis, diabetes mellitus and cancer (*Kurundkar and Thannickal, 2016*; *Ma et al., 2013*; *Ma et al., 2013*; *Di Pietro et al., 2017*; *Saadatian-Elahi et al., 2020*). This suggests that antiviral responses in these individuals could be repressed, leading to impaired control of chronic herpesvirus infections and poor clinical outcomes (*Stowe et al., 2007*; *Ye et al., 2016*).

Structural and functional data prior to our study indicate that STING is oxidized under certain circumstances, but the precise site(s) of oxidation and the role of ROS in STING regulation has been unclear. On one hand, nuclear factor erythroid 2-related factor 2 (NRF2), which drives the expression of antioxidant genes, decreases STING-induced interferon and thus increases susceptibility to herpes simplex virus-2 (HSV-2) (*Gunderstofte et al., 2019*; *Olagnier et al., 2018*). These studies did not indicate whether STING itself is oxidized in the presence or absence of NRF2. On the other hand, induction of oxidative stress by the complex I inhibitor rotenone inhibits ectopically expressed STING activity and interferon production (*Jin et al., 2010*).

The malleable chemistry of cysteines makes them optimal targets for redox regulation (*Bindoli et al., 2008*; *Wang et al., 2012*). Cysteines are susceptible to multiple post-translational modifications, including sulfenylation, SOH; sulfinylation, SO_2H; sulfinylation, SO_3H; glutathionylation, -SSG; protein disulfide formation; nitrosylation, etc., all of which can affect protein structure and function. Moreover, many cysteine oxidative modifications are reversible, making them ideal for initiating and terminating signals. Redox modification can also be either activating or inhibiting for protein function. For example, sulfenylation of the EGFR catalytic site enhances kinase activity whereas oxidation-induced disulfide bond formation inactivates MKK6 (*Paulsen et al., 2012*; *Wani et al., 2011*).

Previous reports indicate that cysteine residues of STING may form disulfide-containing polymers (*Ergun et al., 2019*; *Jin et al., 2010*; *Jønsson et al., 2017*; *Li et al., 2015*; *Motani et al., 2015*). A recent report identified redox regulation of C206 upon cGAMP binding to STING (*Cuervo et al., 2020*). The authors also indicate the C148 may be oxidized under baseline conditions but did not characterize this oxidation. In our report, we identify C148 oxidation of STING as a posttranslational modification that negatively regulates STING activation. Our model suggests that increased ROS promote oxidation of C148. C148 is important for forming disulfide bridges between STING dimers, leading to the formation of stabilized polymers in the ER (*Ergun et al., 2019*; *Shang et al., 2019*). When C148 is oxidized, STING no longer forms stable polymers, thereby preventing recruitment and activation of TBK1 (*Figure 7*; *Zhang et al., 2019*). Notably, our data do not distinguish whether oxidized STING can still bind to cGAMP or if oxidation prevents cGAMP binding and conformational change of STING dimers.

Some pathogens may have evolved to take advantage of ROS to inhibit cellular defenses. Indeed, multiple herpesviruses induce oxidative stress in infected cells and ROS promote virus replication in vitro. Using a mouse model gammaherpesvirus, MHV68, we demonstrated that in vivo treatment of mice with menadione to induce ROS increased virus replication and treatment of mice with NAC to inhibit ROS suppressed virus replication. The effects of menadione and NAC treatments were relatively modest in these in vivo experiments. However, our results are consistent with previous reports that PRRs other than STING also participate in the control of MHV68 infection (*Bussey et al., 2019*; *Sun et al., 2015*). In addition, another group showed that implantation of KSHV-infected cells into mice and treatment with NAC inhibits lytic replication of this human gammaherpesvirus (*Ye et al., 2011*). Further work is required to determine if ROS inhibition of cytoplasmic DNA sensing promotes
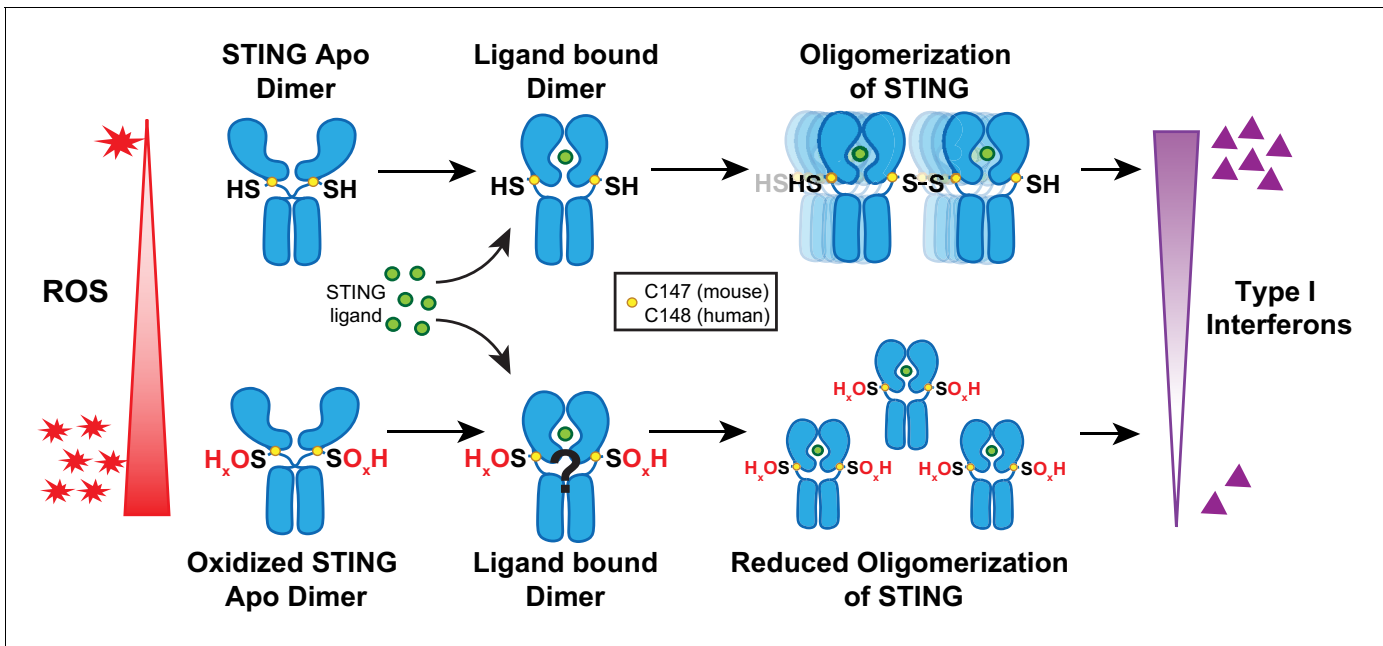
Figure 7. Model of ROS modification of STING. Increasing ROS leads to oxidation of free thiol on C148 of human STING and C147 of mouse STING. This prevents polymerization of STING upon binding of 2',3'-cGAMP and leads to reduced interferon production.

reactivation of herpesviruses from latency in vivo and whether particular herpesvirus-encoded genes alter the ROS levels in the cell.

Consistent with our data that STING undergoes redox modification, a recent study demonstrates that glutathione peroxidase 4 (GPX4), an enzyme that protects cells against membrane lipid peroxidation and maintains redox homeostasis, is required for the activation of the cGAS-STING pathway. This report also shows that GPX4 is required for innate immune responses against herpes simplex virus 1 (*Jia et al., 2020*). These data, along with our data, support a model whereby ROS promote DNA virus acute replication in a STING-dependent manner.

Oxidative inhibition of STING may also be important for preventing overactivation of the interferon response due to other sources of cytosolic DNA, not just viral infection. Mitochondrial damage and release of mtDNA into the cytoplasm activates the cGAS-STING pathway (*Chen et al., 2018*; *McArthur et al., 2018*; *West et al., 2015*). In the absence of cellular caspases, mtDNA induces type I interferon production (*White et al., 2014*). Notably, many of the stimuli that lead to mitochondrial fragmentation and release of mtDNA also produce mitochondrial ROS (*Araujo et al., 2018*; *Willems et al., 2015*; *Woo et al., 2012*). Redox regulation of STING may represent a negative regulatory mechanism to limit aberrant production of type I interferon.

Multiple autoimmune and autoinflammatory diseases are associated with increased production of interferon and are termed type I interferonopathies. These monogenic diseases are driven by mutations in DNases or STING (*Motwani et al., 2019*). Particularly, the rare autoinflammatory disease called STING-associated vasculopathy with onset in infancy (SAVI) is caused by gain-of-function mutations in the gene that encodes STING, *TMEM173* (*Liu et al., 2014*). Of the six patients identified with SAVI, all had point mutations in close proximity to C148, with one patient having a V147L mutation. It is therefore plausible that this region is important for negatively regulating STING activity and normalizing the 'basal' or tonic levels of interferon in cells (*Gough et al., 2012*). We found that NAC treatment of macrophages prior to viral infection increased *Ifnb* transcript levels but did not significantly alter MHV68 growth. The small change in basal ROS with NAC treatment may be insufficient to suppress virus replication. However, changes in the low level of endogenous ROS in cells could regulate basal interferon through STING activation and could contribute interferonopathies over the long term.

Altogether, our results identify a critical post-translational modification of STING and indicate that redox regulation of STING is important for innate immune responses against certain DNA viruses. The cysteine at position 147 in mice and 148 in humans is a critical cysteine for STING polymer formation and activation. Identifying the post-translational modifications of STING contributes not only to our understanding of the basic biology of the cGAS/STING pathway but is also critical for identifying novel immunotherapies to target interferon production.

Materials and methods

Key resources table

Reagent type (species) or resource	Designation	Source or reference	Identifiers	Additional information
Strain, strain background (*Mus musculus*)	C57BL/6J	The Jackson Laboratory	Stock No. 000664	Bred at UTSW facility with IACUC approval
Strain, strain background (*Mus musculus*)	C57BL/6J-*Tmem173*^{gt}/J	The Jackson Laboratory	Stock No. 017537	Bred at UTSW facility with IACUC approval
Strain, strain background (*Mus musculus*)	B6.129S2-*Ifnar1*^{tm1Agt}/J	The Jackson Laboratory	Stock No. 32045	Bred at UTSW facility with IACUC approval
Strain, strain background (*Mus musculus*)	B6.129P2-*Acox1*^{tm1Jkr}/J	The Jackson Laboratory	Stock No. 029747	Bred at UTSW facility with IACUC approval
Cell line (*Herpesviridae, Rhadinovirus*)	Murine gamma herpesvirus 68 (WUSM stain)	ATCC	VR-1465	
Cell line (*Herpesviridae, Rhadinovirus*)	Murine gamma herpesvirus 68-M3FL	Home made *Hwang et al., 2008*		
Cell line (*Mus musculus*)	3T12	ATCC	Cat# ATCC CCL-164; RRID:CVCL_0637	
Cell line (*Homo sapiens*)	293T	ATCC	Cat# ATCC CRL-3216; RRID:CVCL_0063	
Transfected construct (*Homo sapiens*)	STING	GenBank	AVQ94753.1	Express STING into 293T cells
Antibody	Anti-STING (Rabbit polyclonal)	Proteintech	Cat# 19851-1-AP; RRID:AB_10665370	WB (1:1000); IP (1 ug/ml)
Antibody	Anti-STING (Rabbit monoclonal)	Cell Signaling	Cat# 50494S; RRID:AB_2799375	WB (1:1000)
Antibody	Anti-TBK1/NAK (Rabbit monoclonal)	Cell Signaling	Cat# 3504S; RRID:AB_2255663	WB (1:1000)
Antibody	Anti-IRF-3 (Rabbit monoclonal)	Cell Signaling	Cat# 4302S; RRID:AB_1904036	WB (1:1000)
Antibody	Anti-Phospho-TBK1 (Ser172) (Rabbit monoclonal)	Cell Signaling	Cat# 5483S; RRID:AB_10693472	WB (1:1000)
Antibody	Anti-Phospho-IRF-3 (Ser396) (Rabbit monoclonal)	Cell Signaling	Cat# 4947S; RRID:AB_823547	WB (1:1000)
Antibody	Mouse monoclonal anti-SDHA antibody	Abcam	Cat# ab14715; RRID:AB_301433	WB (1:5000)
Antibody	Anti-MHV68 (Rabbit polyclonal)	Home made *Weck et al., 1997*		FACs (1:1000)

Continued on next page

Continued

Reagent type (species) or resource	Designation	Source or reference	Identifiers	Additional information
Antibody	Anti-Rabbit IgG(H+L) secondary antibody, Alexa Fluor 647 (Goat polyclonal)	Thermo Fisher Scientific	Cat# A-21245; RRID:AB_2535813	FACs (1:4000)
Antibody	Anti-Rabbit IgG, Peroxidase (Donkey polyclonal)	Jackson Immuno Research Laboratory	Cat# 711-035-152; RRID:AB_10015282	WB (1:5000)
Antibody	Anti-Mouse IgG, Peroxidase (Goat polyclonal)	Jackson Immuno Research Laboratory	Cat# 115-035-174; RRID:AB_2338512	WB (1:5000)
Antibody	Anti-FITC (Rabbit polyclonal)	Thermo Fisher Scientific	Cat# 71-1900; RRID:AB_2533978	WB (1:2000)
Recombinant DNA reagent	pcDNA 3.1(+) Mammalian Expression Vector (plasmid)	Thermo Fisher Scientific	Cat# V79020	Vector for the expression of human STING
Sequence-based reagent	*Ifnb* forward	This paper	qPCR primers	CAGCTCCAAGAAAGGACGAAC
Sequence-based reagent	*Ifnb* reverse	This paper	qPCR primers	GGCAGTGTAACTCTTCTGCAT
Sequence-based reagent	*Cxcl10* forward	This paper	qPCR primers	TTAACGTCAGGCCAACAGAG
Sequence-based reagent	*Cxcl10* reverse	This paper	qPCR primers	GAGGGAAACCAGGAAAGATAGG
Sequence-based reagent	*Isg15* forward	This paper	qPCR primers	CAGGACGGTCTTACCCTTTCC
Sequence-based reagent	*Isg15* reverse	This paper	qPCR primers	AGGCTCGCTGCAGTTCTGTAC
Sequence-based reagent	*Isg20* forward	This paper	qPCR primers	CCATGGACTGTGAGATGGTG
Sequence-based reagent	*Isg20* reverse	This paper	qPCR primers	CTCGGGTCGGATGTACTTGT
Sequence-based reagent	*Gapdh* forward	This paper	qPCR primers	GGGTGTGAACCACGAGAAATA
Sequence-based reagent	*Gapdh* reverse	This paper	qPCR primers	GTCATGAGCCCTTCCACAAT
Sequence-based reagent	*Gsr* forward	This paper	qPCR primers	CACCGAGGAACTGGAGAATG
Sequence-based reagent	*Gsr* reverse	This paper	qPCR primers	ATCTGGAATCATGGTCGTGG
Sequence-based reagent	*Gclm* forward	This paper	qPCR primers	AATCAGCCCCGATTTAGTCAG
Sequence-based reagent	*Gclm* reverse	This paper	qPCR primers	CGATCCTACAATGAACAGTTTTGC
Sequence-based reagent	C148 forward	This paper	Site direct mutagenesis PCR primers	CTCTGCAGTGCTGAAAA AGGGAATTTCAACGTGGC
Sequence-based reagent	C148A reverse	This paper	Site direct mutagenesis PCR primers	ATCTCAGCTGGGGCCAGG
Commercial assay or kit	Lipofectamine 3000 Reagent	Thermo Fisher Scientific	Cat# L3000008	
Commercial assay or kit	Qiagen RNeasy Mini Kit	Qiagen	Cat# 74104	

Continued on next page

Continued

Reagent type (species) or resource	Designation	Source or reference	Identifiers	Additional information
Commercial assay or kit	SuperScript VILO cDNA Synthesis Kit	Thermo Fisher Scientific	Cat# 11754050	
Commercial assay or kit	PowerUp SYBR Green Master Mix	Thermo Fisher Scientific	Cat# A25776	
Commercial assay or kit	LIVE/DEAD Fixable Dead Cell Stain Kits	Invitrogen	Cat# L34975	
Commercial assay or kit	Q5 Site-Directed Mutagenesis Kit	New England BioLabs	Cat# E0554S	
Chemical compound, drug	DMXAA	InvivoGen	Cat# tlrl-dmx	(1 ug/ml) for macrophages, (2 ug/ml) for fibroblasts
Chemical compound, drug	2'3'-cGAMP	InvivoGen	Cat# tlrl-nacga23	(10 ug/ml)
Chemical compound, drug	ISD	InvivoGen	Cat# tlrl-isdn	(10 ug/ml)
Chemical compound, drug	poly(dA:dT)	InvivoGen	Cat# tlrl-patn-1	(1 ug/ml)
Chemical compound, drug	poly(I:C)	Invivogen	Cat# tlrl-picw	(1 ug/ml)
Chemical compound, drug	D-Luciferin, Potassium Salt	GOLDBIO	Cat# LUCK	(150 mg/kg)
Chemical compound, drug	Menadione	Sigma	Cat# M9429	(10 mg/kg) for mice, concentration for cells were indicated in each experiment
Chemical compound, drug	Hydrogen peroxide solution	Sigma	Cat# 216763	Concentration for cells were indicated in each experiment
Chemical compound, drug	N-Acetyl-L-cysteine	Sigma	Cat# A7250	2 mM for macrophages, 5 mM in drinking water with 2% sucrose
Chemical compound, drug	Iodoacetamide	Sigma	Cat# I1149	100 mM
Chemical compound, drug	N-ethylmaleimide	Sigma	Cat# E3876	50 mM
Chemical compound, drug	Elastase	Worthington	Cat# LS006363	1 mg/ml
Chemical compound, drug	5-(Iodoacetamido) fluorescein	Sigma	Cat# I9271	5 ug/ml
Chemical compound, drug	Diamide	Sigma	Cat# D3648	200 uM
Software, algorithm	GraphPad Prism 8	GraphPad	www.graphpad.com; RRID:SCR_002798	
Software, algorithm	FlowJo software	FlowJo	www.flowjo.com; RRID:SCR_008520	
Software, algorithm	Live Image Software	Perkin Elmer	www.perkinelmer.com; RRID:SCR_014247	

Animals

C57BL/6J, C57BL/6J-*Tmem173*^{gt}/J (*Sauer et al., 2011*), B6.129S2-*Ifnar1*^{tm1Agt}/J (*Muller et al., 1994*), B6.129P2-*Acox1*^{tm1Jkr}/J (*Fan et al., 1996*). were purchased from The Jackson Laboratory. All mice were housed in a specific pathogen-free, double-barrier facility at the University of Texas

Southwestern Medical Center. Mice were maintained and used under a protocol approved by UT Southwestern Medical Center Institutional Animal Care and Use Committee (IACUC).

Chemicals

Menadione, hydrogen peroxide solution, diamide and N-Acetyl-L-Cysteine were purchased from Sigma-Aldrich. Iodoacetamide (IAM), N-Ethylmaleimide (NEM), 5-iodoacetamido-fluorescein (5-IAF) were purchased from Sigma-Aldrich to label free thiols on protein. cGAMP, ISD, DMXAA, poly I:C, poly dA:dT were purchased from Invivogen to induce interferon signaling.

Chemical treatment

A stock solution of menadione was prepared in DMSO at 50 mg/ml, then diluted to different concentrations with culture medium. Cells were treated with menadione by replacing culture medium with fresh medium containing menadione and incubated at 37°C for a duration indicated in each experiment. A stock solution of hydrogen peroxide was prepared in PBS at the concentration of 1 M, then diluted to different concentration with serum-free medium to avoid the decomposition of hydrogen peroxide by residual catalases in FBS. However, the treatment of hydrogen peroxide was conducted in culture medium containing FBS for the flow cytometric quantification of viral growth in BMDMs, in which case, serum is essential to support virus growth.

Cell culture

Bone marrow derived macrophages were differentiated in DMEM (Corning) with 10% FBS (Biowest) supplemented with 1% glutamine (Corning), 1% HEPES (Corning) and 10% CMG14 (*Takeshita et al., 2000*) supernatant for 7 days. 3T12 cells (ATCC, CCL-164, mycoplasma tested) were maintained in DMEM with 5% FBS supplemented with 1% glutamine and 1% HEPES. 293 T cells (ATCC, CRL-3216, mycoplasma tested), fibroblasts overexpressing human STING were maintained in DMEM with 10% FBS. Primary fibroblasts (MEFs) were isolated from embryonic tissue in DMEM with 10% FBS supplemented with 1% glutamine, 1% HEPES, then passed and maintained in the same culture medium for further propagation.

Generation of virus stocks

Murine γ-herpesvirus 68 (WUSM stain) was purchased from ATCC. Murine γ-herpesvirus 68-M3FL was generated as previously reported (*Hwang et al., 2008*). Virus stock was generated in 3T12 cells and aliquots of virus were stored at −80°C.

Virus infection

Fully differentiated BMDMs were seeded on 24 well plates (1.5×10^5 cells per well) or six well plates (10^6 cells per well). Cells were pretreated with mock control or menadione at 8 μM, 4 μM, or 2 μM for 16 hr. The next day, macrophages were infected with MHV68 at MOI = 5. After an hour, cells were washed with PBS twice to remove unabsorbed virus and resuspended in medium with or without treatments. For the viral growth curve, samples were collected at 0 hr, 24 hr, 48 hr, 72 hr and 96 hr after infection and were frozen at −80°C. The titer of virus was determined by plaque assay in 3T12 cells. For qRT-PCR, cells were washed with ice-cold PBS twice at 6 hr after infection and were frozen at −80°C.

Plaque assay

The concentration of virus was quantitated by plaque assay in 3T12 cells. The frozen samples containing virus were thawed in an incubator at 37°C. The samples were serial diluted, then added to a monolayer of 3T12 cells. After an hour of absorption, the cells were then covered with 1% methylcellulose. Plates were incubated at 37°C for 7 days, and the monolayers were stained with 0.1% crystal violet.

Flow cytometry for MHV68 lytic protein positive cells

To determine the percentage of cells that express lytic proteins of MHV68 infection, cells were harvested 24 hr after infection and fixed with 2% formaldehyde. The cells were blocked with 10% mouse serum and 1% Fc block (anti-CD16/32, clone 2.4G2, Tonbo), and then stained with polyclonal

rabbit antibody to MHV68 (1:1000) (*Reese et al., 2014*; *Weck et al., 1997*), followed by secondary goat anti-rabbit Alexa Fluor-647 (Thermo Fisher, Invitrogen, A-21244).

Cell viability assay

Fully differentiated BMDMs were treated with different concentrations of menadione as indicated. Cells were then scraped and collected at different time points and stained with LIVE/DEAD Fixable Near-IR Dead Cell Stain Kit (ThermoFisher Scientific) for 30 min at room temperature in the dark. After washing with PBS, dead cells were identified using flow cytometry.

Transfection

293 T cells were seeded on six well plates. The next day, cells were transfected with WT STING vector or C148A STING vector using Lipofectamine 3000 (Thermo Fisher Scientific) according to the manufacturer's protocol.

Western blot

Cells were lysed with RIPA buffer (150 mM NaCl, 1% NP-40, 0.5% sodium deoxycholate, 0.1% SDS, 25 mM Tris with protease inhibitor cocktail (Roche)). Protein concentrations were determined using the Bradford assay (Bio-Rad). Equal amounts of protein were mixed with 5x loading sample buffer containing 2-Mercaptoethanol and heated at 97°C for seven mins. The samples were resolved by 4–12% Bis-Tris plus gels (Thermo Fisher Scientific) and transferred to a nitrocellulose membrane. Proteins were labeled with primary antibodies against STING (1:1000, Catalogue no.13647S, Cell Signaling; 1:1000, Catalogue no. 1985–1-AP, Proteintech), TBK1 (1:1000, Catalogue no. 3504S, Cell Signaling), IRF3 (1:1000, Catalogue no. 4302S, Cell Signaling), pTBK1 (1:1000, Catalogue no. 5483S, Cell Signaling), pIRF3 (1:1000, Catalogue no. 4947S, Cell Signaling), SDHA (1:5000, Catalogue no. ab14715, Abcam), β-actin (1:5000, Catalogue no. A2228, Sigma). Secondary antibodies used were donkey-anti-rabbit (1:5000, Catalogue no.711-035-152, Jackson ImmunoResearch Laboratory) and goat-anti-mouse peroxidase (1:5000, Catalogue no.115-035-174 Jackson ImmunoResearch Laboratory). Membranes were developed using Luminata Forte Western HRP substrate (Millipore). For non-reducing SDS-PAGE, protein was mixed with 5x loading sample buffer and incubated at RT for 1 hr without boiling. Samples were then resolved by 4–12% Bis-Tris plus gels.

RT-qPCR

Cells were plated in six well plates, either infected with MHV68 or induced with STING ligand as indicated. RNA was extracted using RNeasy Mini Kit (Qiagen) and reverse transcribed into cDNA using SuperScript VILO cDNA Synthesis Kit (Thermo Fisher Scientific). Relative quantification of target genes was determined using PowerUp SYBR Green Master Mix (Thermo Fisher Scientific) in a QuantStudio 7 Flex real time PCR system. Sequences of primers are as follow:

Primers	Sequence
Ifnb forward	CAGCTCCAAGAAAGGACGAAC
Ifnb reverse	GGCAGTGTAACTCTTCTGCAT
Cxcl10 forward	TTAACGTCAGGCCAACAGAG
Cxcl10 reverse	GAGGGAAACCAGGAAAGATAGG
Isg15 forward	CAGGACGGTCTTACCCTTTCC
Isg15 reverse	AGGCTCGCTGCAGTTCTGTAC
Isg20 forward	CCATGGACTGTGAGATGGTG
Isg20 reverse	CTCGGGTCGGATGTACTTGT
Gapdh forward	GGGTGTGAACCACGAGAAATA
Gapdh reverse	GTCATGAGCCCTTCCACAAT
Gsr forward	CACCGAGGAACTGGAGAATG
Gsr reverse	ATCTGGAATCATGGTCGTGG
Gclm forward	AATCAGCCCCGATTTAGTCAG
Gclm reverse	CGATCCTACAATGAACAGTTTTGC

Immunoprecipitation

Cells were lysed with gentle lysis buffer (Cell Signaling) for 15 mins, and then the cell lysate was spun down at 16,000 g for 10 mins. STING antibody (Proteintech) was added into the cell lysate at 1 µg/mL and incubated overnight at 4°C with rotation. The next day, 20 µL of Pierce protein A/G magnetic beads (Thermo Fisher Scientific) were added into each sample and incubated at 4°C for 2 hr to capture STING protein. Samples were then washed with lysis buffer five times, and protein was dissociated from beads by heating at 97°C for seven mins.

STING cloning

FLAG-tagged STING was cloned into pcDNA 3.1 (+) mammalian vector. C148A mutant was generated by site-directed mutagenesis (New England Biolabs). Vectors with wildtype STING and C148A mutated STING were transfected into HEK293T cells for transient STING overexpression. Mutagenesis primers: forward-CTCTGCAGTGCTGAAAAAGGGAATTTCAACGTGGC; reverse-ATCTCAGCTGGGGCCAGG.

Detection of oxidative modification on STING

Sting-/- fibroblasts stably expressing HA-tagged human STING were plated on 10 cm dishes at a density of 10^7 cells per dish. Twenty-four hours later, growth medium with 10% FBS was replaced with DMEM supplemented with 2% FBS. The next day, cells were treated with mock control, 25 µM menadione for 30 mins or 200 µM H_2O_2 for 10 mins in serum-free DMEM. Cells were then washed with ice cold PBS twice and lysed with gentle cell lysis buffer (Cell signaling) containing 5 µM 5-IAF which labels free thiols with a fluorescein (FITC) tag (*Ostman et al., 2011*). Cell lysate was spun down at 16,000 g for 10 mins, and the supernatant was then incubated at RT for 1 hr in the dark. Lysates were subjected to immunoprecipitation for HA-tagged STING and probed for both STING and FITC using western blot.

Mass spectrometry analysis of STING cysteine oxidation

Quantification of cysteine oxidation on STING with mass spectrometry was completed as described previously (*Wu et al., 2020*). Differentiated BMDMs were treated with serum free medium or 25 µM menadione for 30 mins, and proteins were extracted using gentle cell lysis buffer (Cell signaling) with 100 mM iodoactamide to label free thiols (Cys_{red}). After immunoprecipitation, the STING-Trap beads were incubated with alkylation buffer (100 mM iodoacetamide, 2% SDS and 150 mM Tris, PH 8.0) at room temperature for 1 hr to sufficiently label free thiols on STING. Proteins were separated by SDS-PAGE, and the bands corresponding to STING were excised. The protein gel band was digested overnight with elastase (Worthington) following reduction with DTT and a second alkylation step with N-ethylmaleimide to label oxidized thiols (Cys_{ox}). The samples then underwent solid-phase extraction cleanup with an Oasis HLB µElution plate (Waters) and the resulting samples were analyzed by LC-MS/MS, using an Orbitrap Fusion Lumos mass spectrometer (Thermo Electron) coupled to an Ultimate 3000 RSLC-Nano liquid chromatography system (Dionex). Raw MS data files were converted to a peak list format and analyzed using the central proteomics facilities pipeline (CPFP), version 2.0.3 (*Trudgian et al., 2010*; *Trudgian and Mirzaei, 2012*). Peptide identification was performed with a non-specific enzyme search using the Open MS Search Algorithm (OMSSA) (*Geer et al., 2004*) search engine against the mouse protein database from UniProt, with common contaminants and reversed decoy sequences appended (*Elias and Gygi, 2007*). Fragment and precursor tolerances of 10 ppm and 0.5 Da were specified, and three missed cleavages were allowed. Oxidation of Met and carbamidomethylation (iodoacetamide modification) and N-ethylmaleimide modification of Cys were set as variable modifications. Mass spectrometry data were deposited online, with the link of: http://massive.ucsd.edu/ProteoSAFe/status.jsp?task=03fb020e0fe9474ea5fa9326219f7cee.

MHV68 acute replication in mouse

Experiments were carried out using 8–12 weeks old mice under the protocol approved by IACUC. Mice were sex-matched and randomly allocated into groups prior to experiments. For menadione

treatment, mice were injected intraperitoneally with either vehicle control (5% DMSO in corn oil) or menadione (10 mg/kg) for 1 week, starting 3 days before virus infection. For NAC treatment, 5 mM NAC was provided in the water with presence of 2% sucrose that mice were allowed to drink ad libitum throughout the experimental period starting 5 days before infection. Mice were then infected with MHV68-M3FL with a dose of 10^6 PFU by intraperitoneal injection. To quantify virus-encoded luciferase expression (*Hwang et al., 2008*). Mice were weighed and injected with 150 mg/kg of D-Luciferin (GOLDBIO) prior to imaging using an IVIS Lumina III In Vivo Imaging System (PerkinElmer). Total flux (Photons/second) of the abdominal region was determined using Living Image software (PerkinElmer) by designating a circular region of interest (ROI) for each mouse.

Measure transcripts of *Ifnb1* and *Cxcl10* in peritoneal exudate cells (PECs)

Mice aged between 8–12 weeks were sex-matched and randomly allocated into groups prior to experiments. Mice were injected intraperitoneally with either vehicle control (5% DMSO in corn oil) or menadione (10 mg/kg in corn oil) starting 3 days before infection. Mice were then infected with MHV68 at 10^6 PFU by intraperitoneal injection. Twelve hours after infection, PECs from each mouse were collected. RNA was extracted and reverse transcribed. Transcripts of *Ifnb1* and *Cxcl10* were the quantified by qRT-PCR.

Quantification and statistical analysis

Bars are mean ± SE unless otherwise stated in figure legend. Statistical comparisons were performed using GraphPad Prism 7.0 software. *p* value was computed using unpaired one-way or two-way ANOVA. Statistical significance was set at $p < 0.05$. The numbers of independent replicates (n) are reported in the figure legends.

Acknowledgements

Additional information

Funding

Author contributions
Lili Tao, Conceptualization, Data curation, Formal analysis, Validation, Investigation, Visualization, Methodology, Writing - original draft, Writing - review and editing; Andrew Lemoff, Formal analysis, Investigation, Methodology; Guoxun Wang, Investigation, Visualization, Writing - original draft, Writing - review and editing; Christina Zarek, Visualization, Writing - original draft, Writing - review and editing; Alexandria Lowe, Project administration, Writing - review and editing; Nan Yan, Conceptualization, Writing - review and editing; Tiffany A Reese, Conceptualization, Data curation, Supervision, Funding acquisition, Writing - original draft, Project administration, Writing - review and editing

Author ORCIDs
Lili Tao [iD] https://orcid.org/0000-0002-9682-3911
Andrew Lemoff [iD] https://orcid.org/0000-0002-4943-0170
Guoxun Wang [iD] https://orcid.org/0000-0001-9825-3150
Nan Yan [iD] http://orcid.org/0000-0002-0637-3989
Tiffany A Reese [iD] https://orcid.org/0000-0003-2325-6546

Ethics
Animal experimentation: This study was performed in strict accordance with the recommendations in the Guide for the Care and use of Laboratory Animals of the National Institute of Health. Mice were maintained and handled under a protocol approved by UT Southwestern Medical Center Institutional Animal Care and Use Committee (IACUC) protocol number 2015-100990.

Decision letter and Author response
Decision letter https://doi.org/10.7554/eLife.57837.sa1
Author response https://doi.org/10.7554/eLife.57837.sa2

Additional files

Supplementary files
- Source data 1. All source data.
- Transparent reporting form

Data availability
Mass spectrometry data is available at https://doi.org/10.25345/C5MT4W. Source data is available in Prism format.

The following dataset was generated:

Author(s)	Year	Dataset title	Dataset URL	Database and Identifier
Reese T	2020	Reactive Oxygen Species Oxidize STING and Suppress Interferon Production	https://doi.org/10.25345/C5MT4W	MassIVE UCSD, 10.25345/C5MT4W

References

Araujo LF, Siena ADD, Plaça JR, Brotto DB, Barros II, Muys BR, Biagi CAO, Peronni KC, Sousa JF, Molfetta GA, West LC, West AP, Leopoldino AM, Espreafico EM, Silva WA. 2018. Mitochondrial transcription factor A (TFAM) shapes metabolic and invasion gene signatures in melanoma. *Scientific Reports* **8**:14190. DOI: https://doi.org/10.1038/s41598-018-31170-6, PMID: 30242167

Bindoli A, Fukuto JM, Forman HJ. 2008. Thiol chemistry in Peroxidase catalysis and redox signaling. *Antioxidants & Redox Signaling* **10**:1549–1564. DOI: https://doi.org/10.1089/ars.2008.2063, PMID: 18479206

Bottero V, Chakraborty S, Chandran B. 2013. Reactive oxygen species are induced by kaposi's sarcoma-associated herpesvirus early during primary infection of endothelial cells to promote virus entry. *Journal of Virology* **87**:1733–1749. DOI: https://doi.org/10.1128/JVI.02958-12, PMID: 23175375

Bulua AC, Simon A, Maddipati R, Pelletier M, Park H, Kim KY, Sack MN, Kastner DL, Siegel RM. 2011. Mitochondrial reactive oxygen species promote production of proinflammatory cytokines and are elevated in

TNFR1-associated periodic syndrome (TRAPS). *The Journal of Experimental Medicine* **208**:519–533. DOI: https://doi.org/10.1084/jem.20102049, PMID: 21282379

Bussey KA, Murthy S, Reimer E, Chan B, Hatesuer B, Schughart K, Glaunsinger B, Adler H, Brinkmann MM. 2019. Endosomal Toll-Like receptors 7 and 9 cooperate in detection of murine gammaherpesvirus 68 infection. *Journal of Virology* **93**:18. DOI: https://doi.org/10.1128/JVI.01173-18

Chen Y, Zhou Z, Min W. 2018. Mitochondria, oxidative stress and innate immunity. *Frontiers in Physiology* **9**: 1487. DOI: https://doi.org/10.3389/fphys.2018.01487, PMID: 30405440

Chuang YY, Chen Y, Gadisetti , Chandramouli VR, Cook JA, Coffin D, Tsai MH, DeGraff W, Yan H, Zhao S, Russo A, Liu ET, Mitchell JB. 2002. Gene expression after treatment with hydrogen peroxide, Menadione, or t-butyl hydroperoxide in breast Cancer cells. *Cancer Research* **62**:6246–6254. PMID: 12414654

Cuervo NZ, Fortin A, Caron E, Chartier S, Grandvaux N. 2020. Pinpointing of cysteine oxidation sites in vivo by high-resolution proteomics reveals mechanism of redox-dependent inhibition of STING. *bioRxiv*. DOI: https://doi.org/10.1101/2020.03.25.008920

Di Pietro M, Filardo S, Falasca F, Turriziani O, Sessa R. 2017. Infectious agents in atherosclerotic cardiovascular diseases through oxidative stress. *International Journal of Molecular Sciences* **18**:2459. DOI: https://doi.org/10.3390/ijms18112459

Elias JE, Gygi SP. 2007. Target-decoy search strategy for increased confidence in large-scale protein identifications by mass spectrometry. *Nature Methods* **4**:207–214. DOI: https://doi.org/10.1038/nmeth1019, PMID: 17327847

Ergun SL, Fernandez D, Weiss TM, Li L. 2019. STING polymer structure reveals mechanisms for activation, hyperactivation, and inhibition. *Cell* **178**:290–301. DOI: https://doi.org/10.1016/j.cell.2019.05.036, PMID: 31230712

Fan CY, Pan J, Chu R, Lee D, Kluckman KD, Usuda N, Singh I, Yeldandi AV, Rao MS, Maeda N, Reddy JK. 1996. Hepatocellular and hepatic peroxisomal alterations in mice with a disrupted peroxisomal fatty acyl-coenzyme A oxidase gene. *Journal of Biological Chemistry* **271**:24698–24710. DOI: https://doi.org/10.1074/jbc.271.40.24698, PMID: 8798738

Fang FC. 2011. Antimicrobial actions of reactive oxygen species. *mBio* **2**:e00141. DOI: https://doi.org/10.1128/mBio.00141-11, PMID: 21896680

Fisher AB. 2009. Redox signaling across cell membranes. *Antioxidants & Redox Signaling* **11**:1349–1356. DOI: https://doi.org/10.1089/ars.2008.2378, PMID: 19061438

Gao R, Li T, Tan B, Ramos da Silva S, Jung JU, Feng P, Gao S-J. 2018. FoxO1 suppresses kaposi's Sarcoma-Associated Herpesvirus Lytic Replication and Controls Viral Latency. *Journal of Virology* **93**:18. DOI: https://doi.org/10.1128/JVI.01681-18

Geer LY, Markey SP, Kowalak JA, Wagner L, Xu M, Maynard DM, Yang X, Shi W, Bryant SH. 2004. Open mass Spectrometry search algorithm. *Journal of Proteome Research* **3**:958–964. DOI: https://doi.org/10.1021/pr0499491, PMID: 15473683

Gonzalez-Dosal R, Horan KA, Rahbek SH, Ichijo H, Chen ZJ, Mieyal JJ, Hartmann R, Paludan SR. 2011. HSV infection induces production of ROS, which potentiate signaling from pattern recognition receptors: role for S-glutathionylation of TRAF3 and 6. *PLOS Pathogens* **7**:e1002250. DOI: https://doi.org/10.1371/journal.ppat.1002250, PMID: 21949653

Gough DJ, Messina NL, Clarke CJ, Johnstone RW, Levy DE. 2012. Constitutive type I interferon modulates homeostatic balance through tonic signaling. *Immunity* **36**:166–174. DOI: https://doi.org/10.1016/j.immuni.2012.01.011, PMID: 22365663

Gunderstofte C, Iversen MB, Peri S, Thielke A, Balachandran S, Holm CK, Olagnier D. 2019. Nrf2 negatively regulates type I interferon responses and increases susceptibility to herpes genital infection in mice. *Frontiers in Immunology* **10**:2101. DOI: https://doi.org/10.3389/fimmu.2019.02101, PMID: 31555293

Hwang S, Wu TT, Tong LM, Kim KS, Martinez-Guzman D, Colantonio AD, Uittenbogaart CH, Sun R. 2008. Persistent gammaherpesvirus replication and dynamic interaction with the host in vivo. *Journal of Virology* **82**: 12498–12509. DOI: https://doi.org/10.1128/JVI.01152-08, PMID: 18842717

Ishikawa H, Ma Z, Barber GN. 2009. STING regulates intracellular DNA-mediated, type I interferon-dependent innate immunity. *Nature* **461**:788–792. DOI: https://doi.org/10.1038/nature08476, PMID: 19776740

Iyanagi T, Yamazaki I. 1970. One-electron-transfer reactions in biochemical systems V. difference in the mechanism of quinone reduction by the NADH dehydrogenase and the NAD(P)H dehydrogenase (DT-diaphorase). *Biochimica Et Biophysica Acta (BBA) - Bioenergetics* **216**:282–294. DOI: https://doi.org/10.1016/0005-2728(70)90220-3

Jia M, Qin D, Zhao C, Chai L, Yu Z, Wang W, Tong L, Lv L, Wang Y, Rehwinkel J, Yu J, Zhao W. 2020. Redox homeostasis maintained by GPX4 facilitates STING activation. *Nature Immunology* **21**:727–735. DOI: https://doi.org/10.1038/s41590-020-0699-0, PMID: 32541831

Jin L, Lenz LL, Cambier JC. 2010. Cellular reactive oxygen species inhibit MPYS induction of IFNβ. *PLOS ONE* **5**: e15142. DOI: https://doi.org/10.1371/journal.pone.0015142, PMID: 21170271

Jønsson KL, Laustsen A, Krapp C, Skipper KA, Thavachelvam K, Hotter D, Egedal JH, Kjolby M, Mohammadi P, Prabakaran T, Sørensen LK, Sun C, Jensen SB, Holm CK, Lebbink RJ, Johannsen M, Nyegaard M, Mikkelsen JG, Kirchhoff F, Paludan SR, et al. 2017. IFI16 is required for DNA sensing in human macrophages by promoting production and function of cGAMP. *Nature Communications* **8**:14391. DOI: https://doi.org/10.1038/ncomms14391, PMID: 28186168

Kosower NS, Kosower EM. 1995. Diamide: an oxidant probe for thiols. *Methods in Enzymology* **251**:123–133. DOI: https://doi.org/10.1016/0076-6879(95)51116-4, PMID: 7651192

Kurundkar A, Thannickal VJ. 2016. Redox mechanisms in age-related lung fibrosis. *Redox Biology* **9**:67–76. DOI: https://doi.org/10.1016/j.redox.2016.06.005, PMID: 27394680

Li Z, Liu G, Sun L, Teng Y, Guo X, Jia J, Sha J, Yang X, Chen D, Sun Q. 2015. PPM1A regulates antiviral signaling by antagonizing TBK1-mediated STING phosphorylation and aggregation. *PLOS Pathogens* **11**:e1004783. DOI: https://doi.org/10.1371/journal.ppat.1004783, PMID: 25815785

Liu Y, Jesus AA, Marrero B, Yang D, Ramsey SE, Sanchez GAM, Tenbrock K, Wittkowski H, Jones OY, Kuehn HS, Lee CR, DiMattia MA, Cowen EW, Gonzalez B, Palmer I, DiGiovanna JJ, Biancotto A, Kim H, Tsai WL, Trier AM, et al. 2014. Activated STING in a vascular and pulmonary syndrome. *New England Journal of Medicine* **371**: 507–518. DOI: https://doi.org/10.1056/NEJMoa1312625, PMID: 25029335

Loor G, Kondapalli J, Schriewer JM, Chandel NS, Vanden Hoek TL, Schumacker PT. 2010. Menadione triggers cell death through ROS-dependent mechanisms involving PARP activation without requiring apoptosis. *Free Radical Biology and Medicine* **49**:1925–1936. DOI: https://doi.org/10.1016/j.freeradbiomed.2010.09.021, PMID: 20937380

Ma Q, Cavallin LE, Leung HJ, Chiozzini C, Goldschmidt-Clermont PJ, Mesri EA. 2013. A role for virally induced reactive oxygen species in kaposi's sarcoma herpesvirus tumorigenesis. *Antioxidants & Redox Signaling* **18**:80–90. DOI: https://doi.org/10.1089/ars.2012.4584, PMID: 22746102

McArthur K, Whitehead LW, Heddleston JM, Li L, Padman BS, Oorschot V, Geoghegan ND, Chappaz S, Davidson S, San Chin H, Lane RM, Dramicanin M, Saunders TL, Sugiana C, Lessene R, Osellame LD, Chew TL, Dewson G, Lazarou M, Ramm G, et al. 2018. BAK/BAX macropores facilitate mitochondrial herniation and mtDNA efflux during apoptosis. *Science* **359**:eaao6047. DOI: https://doi.org/10.1126/science.aao6047, PMID: 29472455

Motani K, Ito S, Nagata S. 2015. DNA-Mediated cyclic GMP-AMP Synthase-Dependent and -Independent regulation of innate immune responses. *The Journal of Immunology* **194**:4914–4923. DOI: https://doi.org/10.4049/jimmunol.1402705, PMID: 25855353

Motwani M, Pesiridis S, Fitzgerald KA. 2019. DNA sensing by the cGAS-STING pathway in health and disease. *Nature Reviews Genetics* **20**:657–674. DOI: https://doi.org/10.1038/s41576-019-0151-1, PMID: 31358977

Muller U, Steinhoff U, Reis L, Hemmi S, Pavlovic J, Zinkernagel R, Aguet M. 1994. Functional role of type I and type II interferons in antiviral defense. *Science* **264**:1918–1921. DOI: https://doi.org/10.1126/science.8009221

Olagnier D, Brandtoft AM, Gunderstofte C, Villadsen NL, Krapp C, Thielke AL, Laustsen A, Peri S, Hansen AL, Bonefeld L, Thyrsted J, Bruun V, Iversen MB, Lin L, Artegoitia VM, Su C, Yang L, Lin R, Balachandran S, Luo Y, et al. 2018. Nrf2 negatively regulates STING indicating a link between antiviral sensing and metabolic reprogramming. *Nature Communications* **9**:3506. DOI: https://doi.org/10.1038/s41467-018-05861-7, PMID: 30158636

Ostman A, Frijhoff J, Sandin A, Böhmer FD. 2011. Regulation of protein tyrosine phosphatases by reversible oxidation. *The Journal of Biochemistry* **150**:345–356. DOI: https://doi.org/10.1093/jb/mvr104, PMID: 21856739

Paiva CN, Bozza MT. 2014. Are reactive oxygen species always detrimental to pathogens? *Antioxidants & Redox Signaling* **20**:1000–1037. DOI: https://doi.org/10.1089/ars.2013.5447, PMID: 23992156

Paulsen CE, Truong TH, Garcia FJ, Homann A, Gupta V, Leonard SE, Carroll KS. 2012. Peroxide-dependent sulfenylation of the EGFR catalytic site enhances kinase activity. *Nature Chemical Biology* **8**:57–64. DOI: https://doi.org/10.1038/nchembio.736

Reese TA, Wakeman BS, Choi HS, Hufford MM, Huang SC, Zhang X, Buck MD, Jezewski A, Kambal A, Liu CY, Goel G, Murray PJ, Xavier RJ, Kaplan MH, Renne R, Speck SH, Artyomov MN, Pearce EJ, Virgin HW. 2014. Helminth infection reactivates latent γ-herpesvirus via cytokine competition at a viral promoter. *Science* **345**: 573–577. DOI: https://doi.org/10.1126/science.1254517, PMID: 24968940

Saadatian-Elahi M, Bauduceau B, Del-Signore C, Vanhems P. 2020. Diabetes as a risk factor for herpes zoster in adults: a synthetic literature review. *Diabetes Research and Clinical Practice* **159**:107983. DOI: https://doi.org/10.1016/j.diabres.2019.107983, PMID: 31846665

Sauer JD, Sotelo-Troha K, von Moltke J, Monroe KM, Rae CS, Brubaker SW, Hyodo M, Hayakawa Y, Woodward JJ, Portnoy DA, Vance RE. 2011. The N-ethyl-N-nitrosourea-induced goldenticket mouse mutant reveals an essential function of sting in the in vivo interferon response to Listeria monocytogenes and cyclic dinucleotides. *Infection and Immunity* **79**:688–694. DOI: https://doi.org/10.1128/IAI.00999-10, PMID: 21098106

Schieber M, Chandel NS. 2014. ROS function in redox signaling and oxidative stress. *Current Biology* **24**:R453–R462. DOI: https://doi.org/10.1016/j.cub.2014.03.034, PMID: 24845678

Shang G, Zhang C, Chen ZJ, Bai XC, Zhang X. 2019. Cryo-EM structures of STING reveal its mechanism of activation by cyclic GMP-AMP. *Nature* **567**:389–393. DOI: https://doi.org/10.1038/s41586-019-0998-5, PMID: 30842659

Soucy-Faulkner A, Mukawera E, Fink K, Martel A, Jouan L, Nzengue Y, Lamarre D, Vande Velde C, Grandvaux N. 2010. Requirement of NOX2 and reactive oxygen species for efficient RIG-I-Mediated antiviral response through regulation of MAVS expression. *PLOS Pathogens* **6**:e1000930. DOI: https://doi.org/10.1371/journal.ppat.1000930

Stowe RP, Kozlova EV, Yetman DL, Walling DM, Goodwin JS, Glaser R. 2007. Chronic herpesvirus reactivation occurs in aging. *Experimental Gerontology* **42**:563–570. DOI: https://doi.org/10.1016/j.exger.2007.01.005, PMID: 17337145

Sun C, Schattgen SA, Pisitkun P, Jorgensen JP, Hilterbrand AT, Wang LJ, West JA, Hansen K, Horan KA, Jakobsen MR, O'Hare P, Adler H, Sun R, Ploegh HL, Damania B, Upton JW, Fitzgerald KA, Paludan SR. 2015. Evasion of innate cytosolic DNA sensing by a gammaherpesvirus facilitates establishment of latent infection. *The Journal of Immunology* **194**:1819–1831. DOI: https://doi.org/10.4049/jimmunol.1402495, PMID: 25595793

Takeshita S, Kaji K, Kudo A. 2000. Identification and characterization of the new osteoclast progenitor with macrophage phenotypes being able to differentiate into mature osteoclasts. *Journal of Bone and Mineral Research* **15**:1477–1488. DOI: https://doi.org/10.1359/jbmr.2000.15.8.1477, PMID: 10934646

Tanaka Y, Chen ZJ. 2012. STING specifies IRF3 phosphorylation by TBK1 in the cytosolic DNA signaling pathway. *Science Signaling* **5**:ra20. DOI: https://doi.org/10.1126/scisignal.2002521, PMID: 22394562

Trudgian DC, Thomas B, McGowan SJ, Kessler BM, Salek M, Acuto O. 2010. CPFP: a central proteomics facilities pipeline. *Bioinformatics* **26**:1131–1132. DOI: https://doi.org/10.1093/bioinformatics/btq081, PMID: 20189941

Trudgian DC, Mirzaei H. 2012. Cloud CPFP: a shotgun proteomics data analysis pipeline using cloud and high performance computing. *Journal of Proteome Research* **11**:6282–6290. DOI: https://doi.org/10.1021/pr300694b, PMID: 23088505

Tschopp J, Schroder K. 2010. NLRP3 inflammasome activation: the convergence of multiple signalling pathways on ROS production? *Nature Reviews Immunology* **10**:210–215. DOI: https://doi.org/10.1038/nri2725, PMID: 20168318

Van Acker H, Coenye T. 2017. The role of reactive oxygen species in Antibiotic-Mediated killing of Bacteria. *Trends in Microbiology* **25**:456–466. DOI: https://doi.org/10.1016/j.tim.2016.12.008, PMID: 28089288

Virág L, Jaén RI, Regdon Z, Boscá L, Prieto P. 2019. Self-defense of macrophages against oxidative injury: fighting for their own survival. *Redox Biology* **26**:101261. DOI: https://doi.org/10.1016/j.redox.2019.101261, PMID: 31279985

Wang Y, Yang J, Yi J. 2012. Redox sensing by proteins: oxidative modifications on cysteines and the consequent events. *Antioxidants & Redox Signaling* **16**:649–657. DOI: https://doi.org/10.1089/ars.2011.4313, PMID: 21967570

Wani R, Qian J, Yin L, Bechtold E, King SB, Poole LB, Paek E, Tsang AW, Furdui CM. 2011. Isoform-specific regulation of Akt by PDGF-induced reactive oxygen species. *PNAS* **108**:10550–10555. DOI: https://doi.org/10.1073/pnas.1011665108, PMID: 21670275

Weck KE, Dal Canto AJ, Gould JD, O'Guin AK, Roth KA, Saffitz JE, Speck SH, Virgin HW. 1997. Murine gamma-herpesvirus 68 causes severe large-vessel arteritis in mice lacking interferon-gamma responsiveness: a new model for virus-induced vascular disease. *Nature Medicine* **3**:1346–1353. DOI: https://doi.org/10.1038/nm1297-1346, PMID: 9396604

West AP, Brodsky IE, Rahner C, Woo DK, Erdjument-Bromage H, Tempst P, Walsh MC, Choi Y, Shadel GS, Ghosh S. 2011. TLR signalling augments macrophage bactericidal activity through mitochondrial ROS. *Nature* **472**:476–480. DOI: https://doi.org/10.1038/nature09973, PMID: 21525932

West AP, Khoury-Hanold W, Staron M, Tal MC, Pineda CM, Lang SM, Bestwick M, Duguay BA, Raimundo N, MacDuff DA, Kaech SM, Smiley JR, Means RE, Iwasaki A, Shadel GS. 2015. Mitochondrial DNA stress primes the antiviral innate immune response. *Nature* **520**:553–557. DOI: https://doi.org/10.1038/nature14156, PMID: 25642965

White MJ, McArthur K, Metcalf D, Lane RM, Cambier JC, Herold MJ, van Delft MF, Bedoui S, Lessene G, Ritchie ME, Huang DC, Kile BT. 2014. Apoptotic caspases suppress mtDNA-induced STING-mediated type I IFN production. *Cell* **159**:1549–1562. DOI: https://doi.org/10.1016/j.cell.2014.11.036, PMID: 25525874

Willems PH, Rossignol R, Dieteren CE, Murphy MP, Koopman WJ. 2015. Redox homeostasis and mitochondrial dynamics. *Cell Metabolism* **22**:207–218. DOI: https://doi.org/10.1016/j.cmet.2015.06.006, PMID: 26166745

Woo DK, Green PD, Santos JH, D'Souza AD, Walther Z, Martin WD, Christian BE, Chandel NS, Shadel GS. 2012. Mitochondrial genome instability and ROS enhance intestinal tumorigenesis in APC(Min/+) mice. *The American Journal of Pathology* **180**:24–31. DOI: https://doi.org/10.1016/j.ajpath.2011.10.003, PMID: 22056359

Wu F, Chi Y, Jiang Z, Xu Y, Xie L, Huang F, Wan D, Ni J, Yuan F, Wu X, Zhang Y, Wang L, Ye R, Byeon B, Wang W, Zhang S, Sima M, Chen S, Zhu M, Pei J, et al. 2020. Hydrogen peroxide sensor HPCA1 is an LRR receptor kinase in Arabidopsis. *Nature* **578**:577–581. DOI: https://doi.org/10.1038/s41586-020-2032-3, PMID: 32076270

Wu J, Chen ZJ. 2014. Innate immune sensing and signaling of cytosolic nucleic acids. *Annual Review of Immunology* **32**:461–488. DOI: https://doi.org/10.1146/annurev-immunol-032713-120156, PMID: 24655297

Ye F, Zhou F, Bedolla RG, Jones T, Lei X, Kang T, Guadalupe M, Gao SJ. 2011. Reactive oxygen species hydrogen peroxide mediates kaposi's sarcoma-associated herpesvirus reactivation from latency. *PLOS Pathogens* **7**:e1002054. DOI: https://doi.org/10.1371/journal.ppat.1002054, PMID: 21625536

Ye F, Zeng Y, Sha J, Jones T, Kuhne K, Wood C, Gao SJ. 2016. High glucose induces reactivation of latent kaposi's Sarcoma-Associated Herpesvirus. *Journal of Virology* **90**:9654–9663. DOI: https://doi.org/10.1128/JVI.01049-16, PMID: 27535045

Zhang C, Shang G, Gui X, Zhang X, Bai XC, Chen ZJ. 2019. Structural basis of STING binding with and phosphorylation by TBK1. *Nature* **567**:394–398. DOI: https://doi.org/10.1038/s41586-019-1000-2, PMID: 30842653